ANKARA YILDIRIM BEYAZIT UNIVERSITY
GRADUATE SCHOOL OF NATURAL AND APPLIED SCIENCES



SUSTAINABLE DESIGN OF FUTURE WIRELESS COMMUNICATION NETWORKS WITH HIGH-ALTITUDE PLATFORM STATIONS (HAPS)

M.Sc. Thesis by

Mehmet Eren ULUÇINAR

Department of Electrical and Electronics Engineering

May, 2026

ANKARA

SUSTAINABLE DESIGN OF FUTURE WIRELESS COMMUNICATION NETWORKS WITH HIGH-ALTITUDE PLATFORM STATIONS (HAPS)

A Thesis Submitted to the

Graduate School of Natural And Applied Sciences of

Ankara Yıldırım Beyazıt University

In Partial Fulfillment of the Requirements for the Degree of Master of Science in Electrical and Electronics Engineering, Department of Electrical and Electronics Engineering

by

Mehmet Eren ULUÇINAR

May, 2026

ANKARA

M.Sc. THESIS EXAMINATION RESULT FORM

We have read the thesis entitled "**SUSTAINABLE DESIGN OF FUTURE WIRELESS COMMUNICATION NETWORKS WITH HIGH-ALTITUDE PLATFORM STATIONS (HAPS)** " completed by **MEHMET EREN ULUÇINAR** under supervision of **ASST. PROF. DR. METİN ÖZTÜRK** and we certify that in our opinion it is fully adequate, in scope and in quality, as a thesis for the degree of Master of Science.

Asst. Prof. Dr. Metin ÖZTÜRK

Supervisor

Assoc. Prof. Dr. Ahmet AKBULUT

Jury Member

Asst. Prof. Dr. Özgün ERSOY

Jury Member

Prof. Dr. İlyas ÇANKAYA

Director

Graduate School of Natural and Applied Sciences

ETHICAL DECLARATION

I hereby declare that, in this thesis which has been prepared in accordance with the Thesis Writing Manual of Graduate School of Natural and Applied Sciences,

- All data, information and documents are obtained in the framework of academic and ethical rules,
- All information, documents and assessments are presented in accordance with scientific ethics and morals,
- All the materials that have been utilized are fully cited and referenced,
- No change has been made on the utilized materials,
- All the works presented are original,

and in any contrary case of above statements, I accept to renounce all my legal rights.

Date: 2026, 11 May **Signature:** _____

Name & Surname: Mehmet Eren ULUÇINAR

ACKNOWLEDGEMENTS

I would like to express my sincere gratitude to my supervisor, Asst. Prof. Dr. Metin ÖZTÜRK, for his invaluable guidance, continuous support, and insightful feedback throughout this thesis. His expertise and critical perspective have significantly contributed to the development and completion of this work. I am truly grateful for his mentorship.

Furthermore, I would like to extend my sincere thanks to the members of my thesis committee, Assoc. Prof. Dr. Ahmet AKBULUT and Asst. Prof. Dr. Özgün ERSOY, for their insightful evaluations, constructive criticism, and valuable suggestions. Their feedback has significantly improved the quality and clarity of this thesis.

Finally, I would like to sincerely thank my parents for their unconditional love, patience, and unwavering support throughout my life. Without their sacrifices and encouragement, this thesis would not have been possible. I am also grateful to my friends for their continuous support, understanding, and companionship during this process.

I would also like to thank TÜBİTAK for its support through the 2211 (2210-A) National MSc Scholarship Programme.

I am sincerely grateful to TÜBİTAK BİLGEM for its support through the HAPS-COM project, which provided valuable contributions to this research.

May, 2026 **Mehmet Eren ULUÇINAR**

SUSTAINABLE DESIGN OF FUTURE WIRELESS COMMUNICATION NETWORKS WITH HIGH-ALTITUDE PLATFORM STATIONS (HAPS)

ABSTRACT

The evolution of wireless cellular networks toward sixth-generation (6G) systems is driven by the need for ubiquitous connectivity, lower latency, and sustainable operation, making energy efficiency a critical objective for radio access networks (RAN). In this context, cell switching has been widely investigated as an effective technique to reduce energy consumption by switching off underutilized base stations (BSs). To further enhance coverage and connectivity, non-terrestrial networks (NTN), particularly high-altitude platform stations (HAPS) modeled as International Mobile Telecommunications (IMT) BSs (HIBS), are increasingly integrated into terrestrial networks (TN). Although HIBS-assisted cell switching can improve energy efficiency, excessive reliance on HIBS may degrade user performance due to higher path loss and unfavorable propagation conditions, while turning HIBS into a primary traffic carrier. To address this issue, this thesis proposes a propagation- and rate-aware bounded-NTN cell switching framework, where HIBS utilization is explicitly constrained while maintaining user-centric performance. The conventional energy-focused model (EFM) is reformulated as a constrained multi-objective optimization problem considering network power consumption, HIBS utilization, unconnected users, data rate degradation, and fairness. Realistic propagation effects, including building entry loss (BEL) and atmospheric attenuation, are incorporated to reflect NTN-specific channel conditions. The optimization problem is solved using the ϵ-constraint method (ϵCM), enabling a flexible trade-off between energy efficiency and user performance. Results show that the proposed framework reduces HIBS utilization by up to 80% at moderate user densities compared to EFM, mitigates data rate degradation by up to 70% for high-loss indoor users, and achieves up to 15% additional power savings. Finally, a hybrid Python–Sionna–OpenAirInterface (OAI) evaluation demonstrates the practical feasibility of the framework beyond conventional simulation-only studies.

Keywords: NTN, HAPS, HIBS, sustainability, energy-efficiency, 6G, cell switching, propagation awareness.

YÜKSEK İRTİFA PLATFORM İSTASYONLARI (HAPS) İLE GELECEK KABLOSUZ İLETİŞİM AĞLARININ SÜRDÜRÜLEBİLİR TASARIMI

ÖZ

Altıncı nesil (6G) kablosuz hücresel ağlara doğru evrim; her yerde kesintisiz bağlantı, daha düşük gecikme ve sürdürülebilir işletim gereksinimleri tarafından yönlendirilmekte olup, enerji verimliliğini radyo erişim ağları (RAN) için kritik bir hedef haline getirmektedir. Bu bağlamda, hücre anahtarlama (cell switching), düşük yüklü baz istasyonlarının (BS) kapatılması yoluyla enerji tüketimini azaltan etkili bir teknik olarak yaygın şekilde incelenmiştir. Kapsama ve bağlantıyı geliştirmek amacıyla, özellikle Uluslararası Mobil Telekomünikasyon (IMT) baz istasyonları (HIBS) olarak modellenen yüksek irtifa platform istasyonları (HAPS) olmak üzere, karasal olmayan ağlar (NTN) giderek karasal ağlara (TN) entegre edilmektedir. HIBS destekli hücre anahtarlama enerji verimliliğini artırabilse de, HIBS'e aşırı bağımlılık; daha yüksek yol kaybı ve elverişsiz yayılım koşulları nedeniyle kullanıcı performansını düşürebilmekte, ayrıca HIBS'in birincil trafik taşıyıcısına dönüşmesine neden olabilmektedir. Bu sorunu ele almak amacıyla, bu tezde HIBS kullanımının açıkça sınırlandırıldığı ve kullanıcı odaklı performansın korunduğu yayılım ve veri hızı farkındalıklı, sınırlandırılmış NTN tabanlı bir hücre anahtarlama çerçevesi önerilmektedir. Geleneksel enerji odaklı model (EFM), ağ güç tüketimi, HIBS kullanımı, bağlantısız kullanıcı sayısı, veri hızı düşüşü yaşayan kullanıcılar ve adalet metriğini dikkate alan kısıtlı çok amaçlı bir optimizasyon problemine dönüştürülmüştür. Ayrıca, NTN'ye özgü kanal koşullarını yansıtmak amacıyla bina giriş kaybı (BEL) ve atmosferik zayıflama gibi gerçekçi yayılım etkileri modele dahil edilmiştir. Optimizasyon problemi, enerji verimliliği ile kullanıcı performansı arasında esnek bir denge sağlayan ϵ-kısıt yöntemi (ϵCM) ile çözülmüştür. Sonuçlar, önerilen çerçevenin EFM'ye kıyasla orta kullanıcı yoğunluklarında HIBS kullanımını %80'e kadar azalttığını, yüksek kayıplı iç mekân kullanıcıları için veri hızı düşüşünü %70'e kadar azalttığını ve %15'e kadar ek güç tasarrufu sağladığını göstermektedir. Son olarak, Python–Sionna–OpenAirInterface (OAI) tabanlı hibrit değerlendirme, önerilen çerçevenin simülasyona dayalı geleneksel yaklaşımların ötesinde pratik uygulanabilirliğini göstermektedir.

Anahtar kelimeler: NTN, HAPS, HIBS, sürdürülebilirlik, enerji verimliliği, 6G, hücre anahtarlama, yayılım farkındalığı.

CONTENTS

M.Sc. THESIS EXAMINATION RESULT FORM ii
ETHICAL DECLARATION iii
ACKNOWLEDGEMENTS iv
ABSTRACT v
ÖZ vi
NOMENCLATURE xi
LIST OF TABLES xvii
LIST OF FIGURES xviii

CHAPTER 1 – INTRODUCTION 1

1.1 Background on NTN 2
1.2 Background on Sustainable 6G Operation through Cell Switching 4
1.3 Problem Statement 6
1.4 Motivation 7
1.5 Research Objectives 7
1.6 Research Contributions 8
1.7 Thesis Organization 9

CHAPTER 2 – LITERATURE REVIEW 11

2.1 TN-based Cell Switching 11
2.2 NTN-based Cell Switching 13
2.3 Research Gap Analysis 18

CHAPTER 3 – SYSTEM MODEL 19

3.1 Network Model 19
3.2 Mobility Model 20
3.3 Propagation Model 22
3.3.1 Path Loss Model for TN 22
3.3.2 Path Loss Model for NTN 25
3.4 Power Consumption Model 26

3.5 User Allocation 27

CHAPTER 4 – PROBLEM FORMULATION 29

4.1 Conventional Energy-Focused Cell Switching Problem Formulation (EFM) 29
4.2 Multi-Objective Optimization Problem Formulation 35
4.3 ϵ-Constraint Method (ϵCM) 44

CHAPTER 5 – METHODOLOGY 46

5.1 Selection of ϵ Parameters 46
5.2 Cell Switching Algorithms 47
5.2.1 Genetic Algorithm 47
5.2.2 Greedy-Based Cell Switching 49
5.2.3 Exhaustive Search-Based Cell Switching 50

CHAPTER 6 – PERFORMANCE EVALUATION 52

6.1 Performance Metrics 52
6.1.1 Achievable Data Rate 52
6.1.2 Total Network Power Consumption 52
6.1.3 HIBS Utilization 53
6.2 Benchmark Models 53
6.2.1 Baseline Model: EFM 53
6.2.2 SBS Operating Modes 53
6.2.3 Cell Switching Algorithms 54
6.3 Simulation Results 54
6.4 Python–Sionna–OAI-Based Performance Evaluation 63

CHAPTER 7 – CONCLUSION 66

CHAPTER 8 – FUTURE WORK 68

REFERENCES 69

APPENDICES 74

Appendix A – Additional OAI Validation Results. 75

NOMENCLATURE

Roman Letter Symbols

$\mathbf{e}_i$	Unit vector with 1 at position i and 0 elsewhere
$\mathbf{M}(\boldsymbol{\epsilon})$	Performance metrics vector corresponding to a given ϵ configuration
$\mathcal{A}$	Deployment area
$\mathcal{B}$	Set of all base stations
$\mathcal{E}_k$	Candidate set of ϵ values for constraint k
$\mathcal{F}$	Set of feasible solutions satisfying ϵ-constraints
$\mathcal{H}$	Set of HIBS base stations
$\mathcal{J}(\Delta, \Omega)$	Fitness (objective) function used in genetic algorithm
$\mathcal{M}$	Set of macro base stations (MBS)
$\mathcal{P}^{(g)}$	Population of solutions at generation g
$\mathcal{S}$	Set of small base stations (SBS)
$\mathcal{U}$	Set of user equipments (UEs)
A_{gas}	Specific attenuation due to atmospheric gases
A_{rain}	Specific attenuation due to rain
b	Base station index
$b_u^{(\text{a})}$	Serving base station of user u after cell switching
$b_u^{(\text{b})}$	Serving base station of user u before cell switching
$C'(h_{\text{UT}})$	Height-dependent correction factor for LoS probability
D	The number of dissatisfied users
d_u	User dissatisfaction indicator
$d_{\text{2D-out}}$	Horizontal distance between BS and UE
d_{3D}	Three-dimensional distance between BS and UE
d_{slant}	Slant distance between HIBS and UE
F	The degree of unfairness in the achievable rate distribution
f_{GHz}	Carrier frequency in GHz
$f_{u,b}$	Feasibility indicator for user-BS association
g	Generation index in genetic algorithm
H	Number of users associated with HIBS
h_{HIBS}	Altitude of HIBS platform

h_{UT}	Height of user terminal
i	Small base station index
$i^{\star}$	Selected SBS index for switching decision
$I_u^{(\mathrm{a})}$	Interference-plus-noise after cell switching
$I_u^{(\mathrm{b})}$	Interference-plus-noise before cell switching
$J(\boldsymbol{\epsilon})$	Performance vector associated with a given $\boldsymbol{\epsilon}$ configuration
k	Interfering base station index
$L_{\mathrm{BEL,base}}$	Baseline building entry loss
L_{BEL}	Building entry loss
L_{E}	Additional building entry loss
L_{FSPL}	Free space path loss
L_{HIBS}	Total path loss for HIBS link
L_{LoS}	Line-of-sight path loss
L_{NLoS}	Non-line-of-sight path loss
$L_{u,b}$	Path loss between user u and BS b
$L_{u,b}^{(\mathrm{a})}$	Path loss after cell switching
$L_{u,b}^{(\mathrm{b})}$	Path loss before cell switching
N	Population size in genetic algorithm
$N_{\tau,\max}$	Maximum allowed users with latency increase
N_{τ}	Number of users with increased latency
P	Total network power consumption
P_{n}	Noise power
$P_{\mathrm{O},b}$	Operational power of BS b
$P_{\mathrm{S},b}$	Sleep mode power of BS b
$P_{\mathrm{T},b}$	Transmit power of BS b
$P_{b,t}$	Power consumption of BS b at time t
$P_{i,t}$	Power consumption of SBS i at time t
$P_{u,b}$	Received power from BS b to user u
$P_{u,k}$	Interference power from BS k
r	Rain rate
R_E	Earth radius
R_u	Achievable data rate of user u

$R_u^{(\mathrm{a})}$	Data rate after cell switching
$R_u^{(\mathrm{b})}$	Data rate before cell switching
$s_{u,b}^{a}$	Association indicator for HIBS
t	Time index
U	Number of unconnected users
u	User index
v_u	Velocity of user u
$v_{\max}$	Maximum user speed
$v_{\min}$	Minimum user speed
$w_u(t)$	Waypoint of user u
$x_u(t)$	Position of user u at time t
z_u	User connection indicator

Greek Letter Symbols

α	Rain attenuation coefficient depending on frequency and polarization
χ	Total number of user equipments
$\Delta P_i^{(r)}$	Power variation caused by switching off SBS i at iteration r
Δt	Time-step duration in the mobility model
Δ	State vector of SBS ON/OFF decisions
$\Delta^{(r)}$	SBS activation vector at iteration r in greedy algorithm
$\Delta^{\star}(\boldsymbol{\epsilon})$	Optimal SBS activation vector for a given $\boldsymbol{\epsilon}$
$\delta_{i,t}$	Binary ON/OFF state of SBS i at time t
ℓ_u	Latency-worsening indicator for user u
ϵ	General constraint parameter in the ϵ-constraint method
ϵ_D	Maximum allowable number of dissatisfied users
ϵ_F	Maximum allowable unfairness level
ϵ_H	Maximum allowable HIBS utilization
ϵ_U	Maximum allowable number of unconnected users
η_b	Efficiency of base station b
Γ	Total number of small base stations
$\gamma_{u,b}$	Signal-to-interference-plus-noise ratio of user u from base station b
ι_{ref}	Receiver reference sensitivity
$\iota_{u,b}$	Received signal strength from base station b to user u

$\kappa_{i,t}$	Effective transmit power of SBS i at time t
$\lambda_{b,t}$	Load factor of base station b
Ω	State vector of SBS power-level decisions
$\Omega^{(r)}$	Power-level vector at iteration r
$\phi(\rho_{i,t})$	Transmit power scaling factor for SBS i
$\rho_{i,t}$	Discrete power-level state of SBS i
σ_{LoS}	Shadowing under line-of-sight conditions
σ_{NLoS}	Shadowing under non-line-of-sight conditions
τ_u^{a}	User latency after cell switching
τ_u^{b}	User latency before cell switching
θ	Elevation angle of HIBS link
ε	Proximity threshold for waypoint arrival
ζ_b^{T}	Total resource block capacity of base station b
ζ_b^{used}	Used resource blocks at base station b
$\zeta_{\text{per-user}}$	Resource blocks required per user
ζ_{T}	Total available resource blocks
$\zeta_{b,t}$	Number of used resource blocks at base station b and time t
k	Rain attenuation coefficient depending on frequency and polarization (ITU model parameter)

Acronyms

ϵCM	ϵ-constraint method
1G	First-Generation
2G	Second-Generation
3G	Third-Generation
3GPP	3rd Generation Partnership Project
4G	Fourth-Generation
5G	Fifth-Generation
6G	Sixth-Generation
AI	Artificial Intelligence
AR	Augmented Reality
BEL	Building Entry Loss
BS	Base Station

EFM	Conventional Energy-Focused Model
eMBB	Enhanced Mobile Broadband
FL	Federated Learning
FSPL	Free Space Path Loss
GEO	Geostationary Earth Orbit
gNB	Next Generation Node B
HAPS	High Altitude Platform Stations
HIBS	HAPS as an IMT base station
HRLLC	Hyper-Reliable Low-Latency Communication
IMT	International Mobile Telecommunications
IoT	Internet of Things
LEO	Low Earth Orbit
LoS	Line-of-Sight
MBS	Macro Base Station
MEO	Medium Earth Orbit
MIP	Mixed-Integer Programming
mMTC	Massive Machine-Type Communications
NLoS	Non Line-of-Sight
NTN	Non-Terrestrial Networks
OAI	OpenAirInterface
QoS	Quality-of-Service
RAN	Radio Access Network
RB	Resource Block
RL	Reinforcement Learning
RNTI	Radio Network Temporary Identifier
RWP	Random Waypoint
SBS	Small Base Stations
SINR	Signal-to-Interference-Plus-Noise Ratio
SMS	Short Message Service
TN	Terrestrial Networks
UAV	Uncrewed Aerial Vehicles
UE	User Equipment

UMa	Urban Macro
URLLC	Ultra-Reliable Low Latency Communications
vHetNet	Vertical Heterogeneous Network
VR	Virtual Reality

LIST OF TABLES

Table 1.1 Comparison of NTN platforms [1]. 3

Table 2.1 Detailed comparison of existing cell switching studies..... 17

Table 3.1 BEL values for traditional and modern office buildings at different frequencies [2]. 24

Table 3.2 Power parameters of various BS types. 26

LIST OF FIGURES

Figure 1.1 International Mobile Telecommunications (IMT) towards 2030 and beyond (IMT-2030) [3]. 1

Figure 1.2 A multi-layer NTN architecture, consisting of satellites, HAPS, and UAV. 3

Figure 1.3 Cell switching in a HIBS-assisted network with traffic offloading from switched-off BSs. 5

Figure 3.1 Multi-layer network model containing HIBS, MBS, SBSs. 19

Figure 3.2 High-loss, low-loss indoor and outdoor users. 21

Figure 4.1 Illustration of SBS operating modes and their impact on coverage and HIBS offloading. 32

Figure 6.1 SBS transmit power scaling. 55

Figure 6.2 Total network power consumption of the ϵCM method with three different methodologies (i.e., genetic algorithm, greedy approach, and exhaustive search). 56

Figure 6.3 Achievable data rate of EFM under varying BEL conditions. 57

Figure 6.4 Achievable data rate of ϵCM under varying BEL conditions. 58

Figure 6.5 Total power consumption of EFM under different user densities. 60

Figure 6.6 Total power consumption of ϵCM under different user densities. 61

Figure 6.7 Number of users connected to HIBS under the EFM and ϵCM frameworks. 62

Figure 6.8 User distribution across BSs before and after cell switching in the simplified Python–Sionna–OAI framework. 64

Figure A.1 OAI gNB logs before and after cell switching, illustrating UE reassociation and connection preservation in the proposed framework. 75

CHAPTER 1

INTRODUCTION

Wireless communication networks have evolved through multiple generations. The first-generation (1G) of wireless networks was developed during the early 1980s with the primary purpose of enabling voice communications. With the introduction of second-generation (2G) networks, communication transitioned into digital form, which improved voice quality and enabled services such as Short Message Service (SMS). Third-generation (3G) networks supported mobile data and Internet access over mobile networks, while the fourth-generation (4G) further advanced these capabilities by enabling mobile broadband Internet, providing higher data rates and supporting streaming services and real-time applications. Subsequently, fifth-generation (5G) mobile broadband systems were designed to support enhanced mobile broadband (eMBB), ultra-reliable low-latency communications (URLLC), and massive machine-type communications (mMTC) [4].

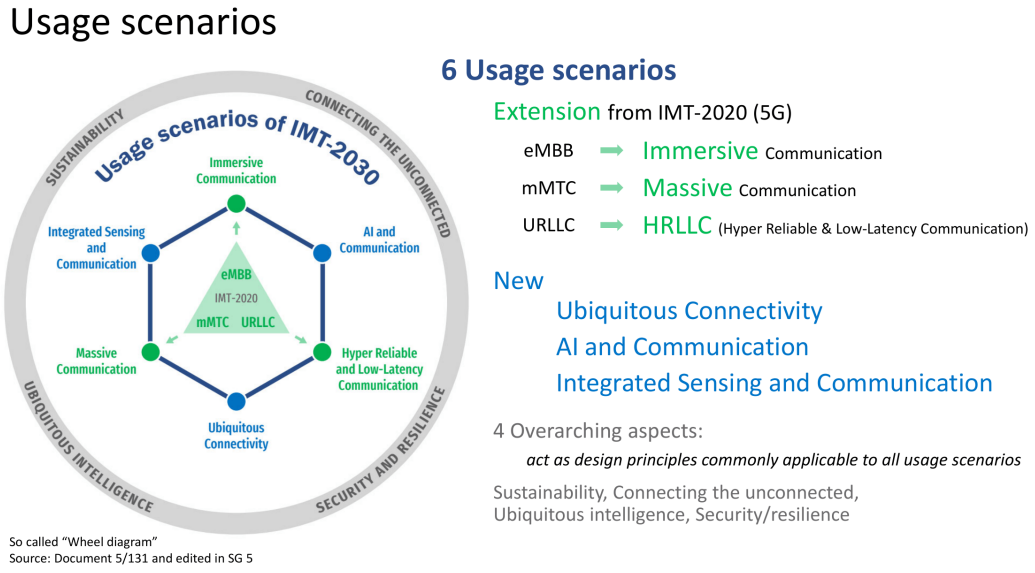


Figure 1.1 International Mobile Telecommunications (IMT) towards 2030 and beyond (IMT-2030) [3].

More recently, features such as immersive communication, ubiquitous connectivity,

and hyper-reliable low-latency communication (HRLLC) have been identified as key objectives of sixth-generation (6G) networks, as illustrated in Fig. 1.1. Notably, non-terrestrial networks (NTN) are expected to play a central role in achieving these objectives by enabling seamless global coverage and extended connectivity. At the same time, sustainability has emerged as a key aspect of 6G, emphasizing the need for energy-efficient and environmentally conscious network operation [3].

Taken together, these developments indicate that future network architectures need to move beyond standalone terrestrial designs toward fully integrated terrestrial networks (TN)–NTN systems that support efficient and sustainable operation [5].

1.1 Background on NTN

NTN describe communication architectures that extend conventional ground-based connectivity by integrating aerial and orbital platforms into the TN. Wider and promising NTN deployments include satellites; namely, low Earth orbit (LEO), medium Earth orbit (MEO), and geostationary Earth orbit (GEO), high-altitude platform stations (HAPS), and uncrewed aerial vehicles (UAV), which have varying characteristics in terms of coverage area, latency, and deployment time flexibility, as summarized in Table 1.1 [1]. Satellites provide wide coverage, but their high orbital altitude leads to long signal propagation delays due to the large transmission distance (e.g., typical altitudes of ~500–2000 km for LEO, ~8000–20000 km for MEO, and ~35786 km for GEO, with corresponding coverage footprints on the order of ~1000–3000 km diameter for LEO, ~10000–12000 km for MEO systems, and up to nearly one-third of the Earth's surface for GEO satellites), resulting in significantly different coverage and latency characteristics [1]. On the other hand, HAPS operate at significantly lower altitudes compared to satellites (typically around ~20 km), enabling much shorter transmission distances and therefore lower propagation delays, which allows faster communication with reduced latency [6]. UAVs operate at much lower altitudes, which further reduces latency and enables fast and flexible deployment [7]. These platforms are mainly used to provide wide-area coverage in rural, maritime, remote, or disaster-affected regions where terrestrial infrastructure is

Table 1.1 Comparison of NTN platforms [1].

Feature	UAV	HAPS	Satellites
Coverage Area	Small	Large	Very Large
Mobility	High	Almost Stationary	Very High
Latency	Low	Moderate	High
Sustainability	Low	High	Moderate
Service Duration	Limited	Long	Very Long
Enable TN BSs Sleep	Limited	High	Limited

limited or unavailable. In 6G networks, NTN is expected to operate together with terrestrial systems to support seamless global connectivity and extend coverage beyond traditional network boundaries [7].

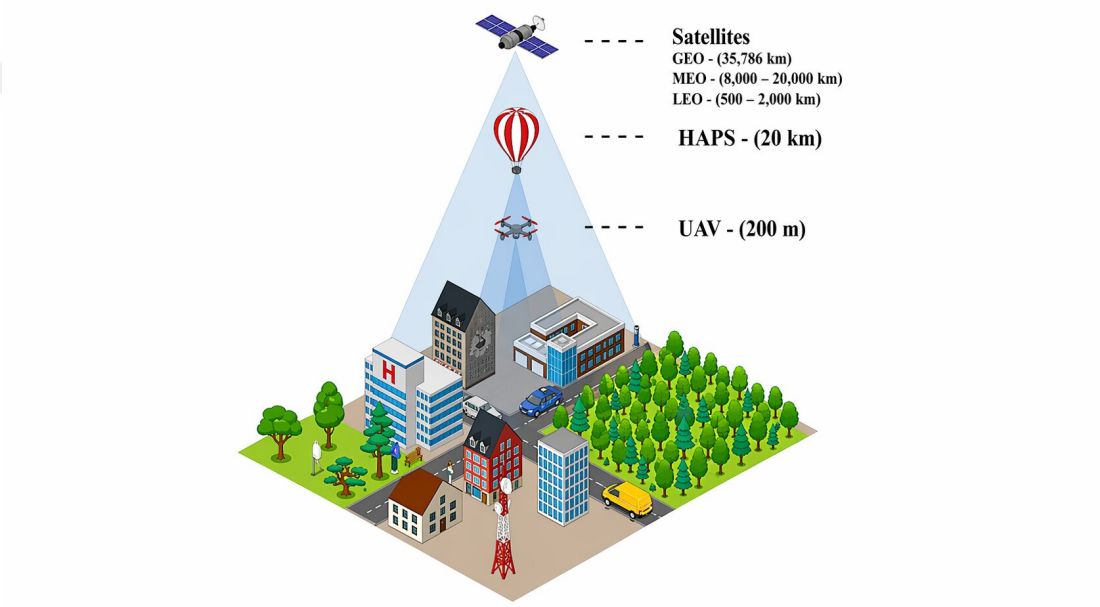


Figure 1.2 A multi-layer NTN architecture, consisting of satellites, HAPS, and UAV.

HAPS experience lower round-trip latency and reduced Doppler sensitivity compared with satellites, while providing significantly greater coverage and service duration than UAVs, making it a promising candidate for deployment in wireless networks [8]. A HAPS as an IMT base station (BS), referred to as (HIBS), is typically deployed at an altitude of approximately 20 km and operates in a quasi-stationary position [6, 9, 10]. These properties enable seamless integration with TN infrastructures and allow HIBS to complement and mitigate for ground network limitations, particularly in rural and remote regions as well as in disaster scenarios where terrestrial infrastructure may be partially or completely unavailable. Moreover, the integration of HIBS with TN supports energy-efficient network operation by enabling dynamic traffic management

and adaptive infrastructure utilization.

1.2 Background on Sustainable 6G Operation through Cell Switching

Sustainability has become a key design objective in wireless networks, driven by the increasing environmental impact and operational costs of large-scale communication infrastructures [3]. In the context of 6G, sustainability includes several aspects such as energy efficiency, carbon emission reduction, and efficient resource utilization [11]. Among these, energy efficiency is especially important in radio access networks (RAN), as BSs consume a significant portion of the total network energy [12]. Therefore, improving energy efficiency in RAN operations has emerged as a key research direction for enabling sustainable 6G networks.

The rapid growth in the number of connected devices, such as the Internet of things (IoT), along with increasing data rate demands, driven by emerging applications such as 4K/8K video streaming, augmented and virtual reality (AR/VR), cloud gaming, and immersive communication services, has led to a significant increase in mobile traffic [13]. Since existing RAN architectures are insufficient to meet the growing demand, network densification, i.e., increasing the number of BSs, is one of the most effective solutions [14]. Although densification can enhance achievable data rates and improve service continuity, it also increases the energy consumption of the RAN [12]. In practice, traffic loads present spatio-temporal variations and therefore it is highly likely that many of these BSs remain underutilized during certain periods, resulting in inefficient energy use. The problem is especially pronounced in dense urban scenarios, where multiple BSs remain concurrently active to guarantee coverage, regardless of instantaneous traffic load. Maintaining a large number of active BSs beyond actual traffic requirements inevitably increases energy consumption, thereby challenging the pursuit of more sustainable 6G networks.

One practical method to reduce energy consumption is to switch off BSs that are idle or underutilized, a technique commonly referred to as cell switching [15, 16], as illustrated in Fig. 1.3. For a BS to be switched off, certain requirements must be satisfied, such as

the presence of another BS with enough capacity to accommodate the offloaded traffic. In TN, cell switching can be applied by offloading the traffic of lightly-loaded or idle BSs to nearby TN BSs. However, this approach is limited by the coverage and capacity of neighboring BSs, particularly in dense or highly dynamic traffic scenarios. As a result, excessive offloading may lead to congestion, degraded user performance, and reduced service reliability. To address these limitations, the integration of HIBS introduces an additional offloading option for switched-off BSs. This enables more lightly-loaded or idle BSs to be turned off, leading to a reduction in total energy consumption. Despite this advantage, the introduction of HIBS also changes the underlying propagation conditions experienced by users after cell switching.

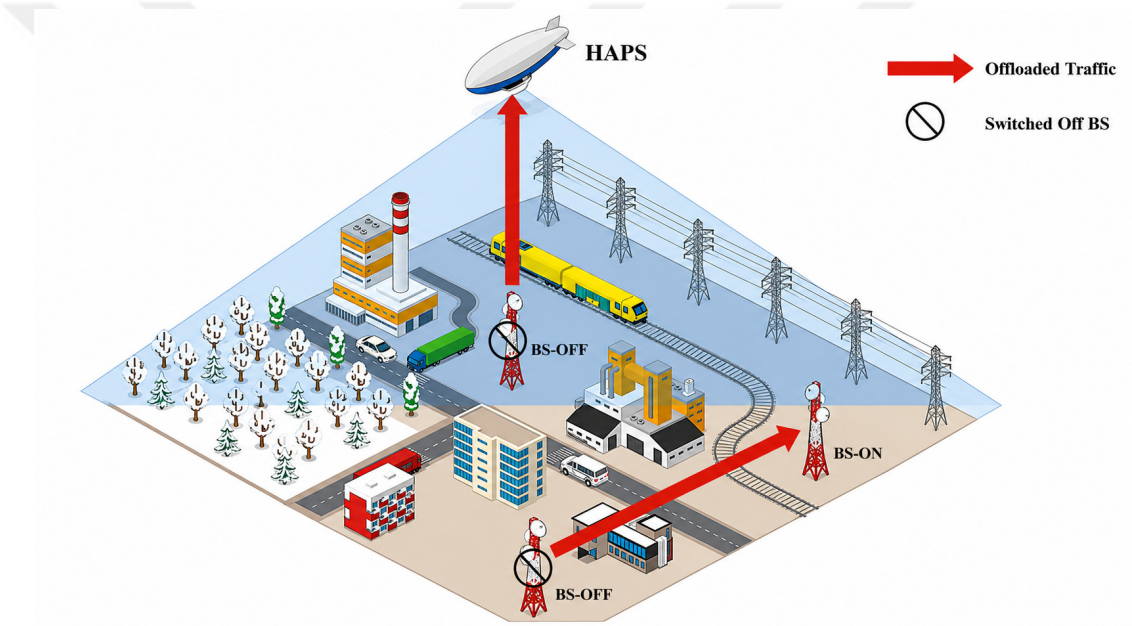


Figure 1.3 Cell switching in a HIBS-assisted network with traffic offloading from switched-off BSs.

On the other hand, when traffic is offloaded to the HIBS, users experience increased path loss due to the long slant distance of the HIBS-user equipment (UE) link and additional atmospheric losses, i.e., gas and rain attenuation. These impairments result in a reduced received signal strength, which can degrade the achievable data rates. In other words, even though HIBS expand coverage and reduce power consumption by allowing more BSs to be switched off, users offloaded to the HIBS may experience degraded performance. This performance degradation becomes more pronounced as reliance on HIBS increases, since more users are offloaded to HIBS under aggressive cell switching. As a result, uncontrolled reliance on HIBS for traffic offloading may lead to excessive

utilization of non-terrestrial resources, turning HIBS from a complementary support layer into a primary traffic carrier, thereby negatively affecting both energy efficiency and user performance.

1.3 Problem Statement

The evolution of wireless cellular networks toward 6G systems introduces new requirements for energy efficiency, user-centric performance, and seamless integration of TN–NTN. In this context, cell switching is an effective approach to reducing energy consumption by switching off underutilized BSs. However, the integration of HIBS, fundamentally changes the operational dynamics of such systems.

Although HIBS-assisted cell switching can significantly improve energy efficiency and coverage, it also introduces important challenges. In particular, excessive reliance on HIBS may lead to performance degradation due to unfavorable propagation conditions, including higher path loss and atmospheric attenuation. Moreover, uncontrolled HIBS utilization can offload traffic from the terrestrial layer to the non-terrestrial layer, potentially increasing overall energy consumption and reducing the effectiveness of cell switching.

Existing studies on energy-efficient cell switching mainly focus on minimizing total network power consumption, often overlooking user-centric performance metrics and the controlled use of NTN resources. As a result, these approaches may lead to unfavorable outcomes, such as an increased number of unconnected users, reduced data rates, and unfair resource distribution among users. Furthermore, most existing studies do not explicitly account for realistic propagation effects, such as building entry loss (BEL), which reduces their applicability in practical scenarios.

Therefore, there is a clear need for a systematic framework that improves energy efficiency while ensuring controlled HIBS utilization and maintaining user-centric performance. Specifically, the challenge is to design a cell switching mechanism that balances power consumption with connectivity, data rate, and fairness, while limiting excessive reliance on non-terrestrial resources under realistic propagation conditions.

1.4 Motivation

The motivation of this thesis stems from the need to design sustainable wireless networks that can reduce energy consumption without compromising user-centric performance. Although switching off underutilized terrestrial BSs reduces energy consumption, it becomes more challenging in TN–NTN architectures. In such cases, using HIBS for cell switching may reduce power consumption but can also lead to weaker propagation conditions, higher path loss, and data rate degradation.

This trade-off is especially critical for indoor users, as their signal quality is highly affected by BEL. In addition, without explicit control of HIBS utilization, the non-terrestrial layer may become overused, reducing its effectiveness as a complementary network layer. As a result, HIBS-assisted cell switching should balance power minimization with connectivity, data rate performance, fairness, and controlled NTN usage.

Motivated by these challenges, this thesis develops a propagation- and rate-aware bounded-NTN cell switching framework that aims to achieve a balanced operation between energy efficiency and user-centric performance in future integrated TN-NTN systems.

1.5 Research Objectives

The objective of this thesis is to develop a cell switching framework for HIBS-assisted TN–NTN networks that improves energy efficiency while preserving user-centric performance. In particular, this work addresses the limitations of existing energy-focused approaches by incorporating realistic propagation conditions and controlling the use of non-terrestrial resources. The proposed framework aims to minimize total network power consumption while constraining the number of unconnected users, data rate degradation, fairness, and HIBS utilization. This allows for a controlled trade-off between energy efficiency and user-centric performance within a unified design.

1.6 Research Contributions

Most cell switching studies focus on reducing network power consumption and represent users mainly through aggregate traffic load. However, this overlooks the strong influence of the surrounding environment on radio conditions, which can lead to inaccurate decisions about switching off certain BSs. To address this limitation, this thesis incorporates environmental factors that directly influence signal propagation into cell switching analysis. In particular, environmental propagation dynamics are captured through BEL, which models signal attenuation due to penetration through different construction materials.

Following cell switching, the BS offering the highest received signal strength may be switched off, resulting in users being offloaded to alternative BSs with weaker received signals. This effect becomes more noticeable when users are offloaded to HIBS, where additional atmospheric losses and higher BEL, especially for indoor users, can significantly reduce the received signal strength. As a result, both user connectivity and achievable data rates are negatively affected after cell switching. Moreover, excessive reliance on HIBS for traffic offloading can lead to excessive use of non-terrestrial resources, offloading a large portion of the network load to HIBS and effectively turning it into a primary traffic carrier rather than a complementary support layer.

To address these challenges, this thesis proposes a propagation-aware and user-centric cell switching framework with controlled HIBS utilization. The conventional energy-focused cell switching (EFM) problem is reformulated as a multi-objective optimization framework that jointly considers energy efficiency and user-centric performance metrics. Within this framework, the ϵ-constraint method (ϵCM) is used to solve the formulated problem. The main contributions of this thesis are summarized as follows:

- The effects of key propagation losses, including BEL and atmospheric losses, on the cell switching performance are analytically derived.
- The EFM is reformulated within the proposed propagation- and rate-aware

bounded-NTN framework as a constrained multi-objective optimization model, where NTN utilization is explicitly bounded through predefined constraints.

- An ϵ-constrained method (ϵCM) is proposed to solve the formulated multi-objective optimization problem, in which connectivity, data rate, fairness, and HIBS utilization are incorporated as constraints within the EFM framework, where HIBS usage is explicitly bounded through predefined constraints to prevent excessive reliance on non-terrestrial resources while ensuring energy efficiency.
- A hybrid framework combining large-scale simulations with Python–Sionna–OpenAirInterface (OAI) emulation is developed to demonstrate the practical feasibility and real-world applicability of the proposed approach, which is rarely addressed in the literature.

To the best of the author's knowledge, this thesis introduces the first bounded-NTN cell switching framework that explicitly limits excessive reliance on HIBS while maintaining energy efficiency and service performance. Within this framework, the EFM is reformulated as a constrained multi-objective optimization model incorporating connectivity, achievable data rate, fairness, and regulated HIBS utilization. Furthermore, the framework incorporates key propagation parameters, such as BEL and atmospheric attenuation, enabling the analysis of their impact on cell switching decisions and user performance.

1.7 Thesis Organization

The remainder of this thesis is organized as follows. Chapter 2 presents a comprehensive literature review, including TN-based and NTN-based cell switching approaches, followed by a detailed research gap analysis. Chapter 3 introduces the system model, including the network architecture, propagation models, power consumption model, and user association framework. Chapter 4 formulates the EFM and introduces the proposed multi-objective optimization framework based on the ϵCM. Chapter 5 presents the methodology, including the implementation of the ϵCM and the cell switching algorithms used to solve the optimization problem. Chapter 6

provides the performance evaluation of the proposed approach, including MATLAB-based system-level simulations and Python–Sionna–OAI based implementation to demonstrate practical applicability. Finally, Chapter 7 concludes the thesis and summarizes the main findings, while Chapter 8 outlines potential directions for future research.

CHAPTER 2

LITERATURE REVIEW

The literature on cell switching can be categorized into two main groups: conventional TN–based cell switching approaches and studies that incorporate NTN components, with a particular focus on HIBS.

2.1 TN-based Cell Switching

Early work in this area was primarily in TN and focused on improving energy efficiency for cellular networks via cell switching. The paper in [17] presents a general review of green cellular networking, emphasizing the growing awareness of environmental issues such as climate change and the rising operational costs of network infrastructures. The study demonstrates that cell switching is a practical solution for improving energy efficiency. However, it also emphasizes that neglecting traffic load dependent effects may result in overestimating the potential energy savings.

Following this early review study, several works have focused on developing practical cell switching mechanisms. The study in [18] examines the increasing energy consumption of cellular networks due to rising demand for mobile services and considers cell switching as a practical solution for improving energy efficiency. Unlike many existing approaches that mainly focus on energy savings, the study also considers spectrum efficiency and user quality-of-service (QoS). To this end, the authors propose an enhanced cell switching method that reallocates radio resources after BSs are switched off, maintaining both energy efficiency and user performance. Simulation results show that the proposed approach not only reduces overall energy consumption but also improves spectrum efficiency compared to baseline methods.

In addition to these general observations, more detailed studies have investigated specific cell switching strategies. The work in [12] investigates cell switching as an energy-efficient solution for next-generation cellular networks, particularly under increasing traffic demand and dense BS deployments. Although network densification

enhances coverage and capacity, it also increases overall energy consumption, raising both environmental and economic concerns. In this context, the study highlights that the design of switching strategies becomes more complex in 5G systems due to advanced physical layer techniques and heterogeneous network architectures. The paper reviews existing switching mechanisms, along with their technical challenges and open research issues related to efficient and reliable cell switching.

In addition to these approaches, more advanced optimization-based methods have been proposed. The paper presented in [19] addresses dynamic cell switching as a practical approach to reduce energy consumption in wireless cellular networks. It formulates the switching problem as an energy minimization task, showing that it is combinatorial and leads to challenges in both computational complexity and signaling overhead. The approach sequentially switches off BSs to minimize network impact, using a metric that captures the additional load on neighboring BSs. To further reduce signaling and implementation overhead, several heuristic versions of the algorithm are introduced based on approximate impact estimation. The results demonstrate that the proposed methods can achieve significant energy savings while maintaining network performance, based on simulations with realistic traffic conditions.

Following these approaches, analytical and scheduling-based strategies have also been investigated. The work in [20] investigates cell switching for energy efficiency, incorporating BS sleep mode at low-traffic periods. This provides continuous coverage through neighboring operational BSs, especially in high-density urban environments. An optimal switching time for each BS's operation is determined based on traffic levels which vary over the course of the day using an analytical model. The results show that significant energy savings can be achieved depending on traffic patterns. The analysis is further extended to heterogeneous networks, where switching decisions follow the traffic load distribution, with less-loaded cells being turned off first. Overall, the study provides practical insights into traffic-aware cell switching strategies for improving energy efficiency in cellular networks.

Despite these advantages, such approaches also reveal important limitations in terms of network performance. The study in [21] shows that although switching off BSs

can provide significant energy savings, improperly designed switching strategies may cause coverage degradation. As a result, the work indicates that jointly considering scheduling and on/off switching strategies is essential for energy-efficient and reliable operation.

To address these challenges, more intelligent and learning-based approaches have been introduced. In this context, the work presented in [15] proposes a reinforcement learning (RL)-based method for selecting when to switch cells in ultra-dense TN cellular networks. The study shows that learning-based cell switching can reduce energy consumption while maintaining user QoS in highly dense deployments.

In addition to conventional RL approaches, more advanced learning-based methods have been proposed to improve scalability, privacy, and decision accuracy. The study [22] proposes a federated learning (FL) and actor–critic based framework for energy-efficient cell switching in ultra-dense 6G networks. The approach uses FL to predict traffic loads, reducing signaling overhead and preserving data privacy, and then applies a modified RL algorithm to determine optimal switching decisions. Although the framework achieves notable energy savings under QoS constraints, it does not consider non-terrestrial integration, propagation effects, or controlled use of aerial platforms.

2.2 NTN-based Cell Switching

Although there has been a lot of improvement with cell switching recently, TN-only methods are still limited with respect to coverage and capacity, particularly in dense or highly dynamic traffic scenarios. To address these limitations, recent studies have explored extending cell switching frameworks by integrating NTNs. These approaches improve coverage, enhance flexibility, and enable traffic offloading by using aerial and satellite platforms. The work in [8] investigates the integration of satellite networks, HIBS and UAVs, into the cell switching framework. By using artificial intelligence (AI)-driven decision-making and resource allocation, the authors show that their multi-layered framework improves load balancing and enables more energy-efficient operation by distributing traffic across different network tiers.

The study presented in [23] investigates the role of UAV-assisted cell switching in improving energy efficiency in 6G networks. Rather than assuming UAV deployment is always beneficial, the authors develop an analytical framework to determine when UAVs can reduce total network energy consumption. The framework considers key factors such as user density, available UAV resources, and service time, while jointly modeling the energy consumption of terrestrial BSs and the UAV. The results show that UAV-assisted switching improves energy efficiency and QoS within certain thresholds. Beyond these limits, however, the additional energy use of the UAV can outweigh its benefits.

Within the NTN context, HIBS are well suited for supporting cell switching operations due to their strong coverage and capacity. Several studies investigate the use of HIBS as a complementary layer to support TN. The authors in [24] analyze an urban RAN scenario and show that offloading part of the traffic to HIBS can reduce the energy demand of ground-based nodes while preserving acceptable QoS levels. Similarly, the study in [25] examines HIBS as an energy-efficient complement in dense urban deployments where further infrastructure expansion is constrained. The proposed approach reduces grid energy consumption and operational costs through adaptive allocation of HIBS capacity, while improving energy efficiency and QoS in future 6G networks.

In a related direction, the authors in [26] examine the growing energy demand of RANs driven by dense deployments and dynamic traffic patterns. Instead of adding more communication infrastructure, the study considers HIBS support and shows that it can handle unpredictable traffic more effectively while improving overall network sustainability.

Beyond traffic offloading, several works integrate HIBS into cell switching frameworks. This work [27] investigates a vertical heterogeneous network (vHetNet) architecture that combines HIBS with terrestrial macro BS (MBS) and small BSs (SBSs) in dense urban environments. The proposed approach improves energy efficiency through traffic-aware cell switching across network layers by allowing SBSs to enter sleep mode while utilizing the additional capacity of HIBS. The results indicate that this approach can

substantially reduce grid power consumption without compromising QoS.

Similarly, [28] analyzes the limitations of conventional terrestrial cell switching approaches under capacity and infrastructure constraints. Integrating HIBS into the framework provides additional coverage and capacity, enabling more flexible switching decisions and reducing energy consumption without compromising QoS.

Compared with many existing studies that primarily focus on energy-efficient HIBS-assisted cell switching, there has been little study concerning the latency aspects of HIBS. Addressing this gap, a delay-aware perspective is introduced in [29], where HIBS is integrated into a cell switching framework that explicitly accounts for user latency constraints. A lightweight Q-learning–based solution is developed to address the resulting optimization problem, and the results under various interference and delay scenarios show effective energy savings while preserving acceptable QoS performance.

The study presented in [30] investigates the role of HIBS in improving the energy efficiency of RAN for future 6G systems. Using simulations based on real traffic patterns, HIBS-assisted RAN are compared with conventional terrestrial deployments. The findings indicate that the wide coverage and self-sustaining operation of HIBS enable notable energy savings and provide valuable design insights for energy-aware 6G network optimization.

While HIBS-assisted cell switching improves energy efficiency, proactive switching decisions introduce new challenges related to traffic load variability. The paper [31] addresses the problem of cell load estimation in HIBS-assisted cell switching schemes, where future traffic conditions cannot be known with certainty. Since switching decisions are taken proactively, estimation errors may lead to suboptimal decisions and reduced energy efficiency. To mitigate this issue, two Q-learning–based approaches with different computational complexities are proposed, and the results show that estimation errors significantly affect switching performance, while learning-based solutions achieve near-optimal performance.

Focusing on the limitations of traffic-awareness in cell switching, recent studies have investigated the role of traffic load estimation and prediction in HIBS-assisted vHetNets.The work in [32] investigates traffic load estimation and prediction in HIBS-assisted vHetNets, addressing the lack of reliable load information for sleeping SBSs. The study incorporates both spatial interpolation-based estimation and spatiotemporal prediction techniques using real-world traffic data, while also accounting for the impact of estimation inaccuracies on cell switching decisions. The results highlight that accurate and robust traffic modeling is essential for enabling practical and energy-efficient cell switching.

The paper in [33] proposes a two-phase framework for energy-efficient cell switching in 6G vHetNets integrating terrestrial BSs and HIBS. In stage one, the authors utilize data driven models to predict the amount of traffic generated by idle SBSs, which is an important aspect of all previous research. In the second phase, these estimates are integrated into a renewable-aware switching strategy that considers for solar-powered SBSs. The results show that accurate load estimation and renewable integration can significantly improve energy efficiency without compromising QoS.

A vHetNet architecture is examined in [34], in which HIBS complements terrestrial MBS and SBSs. The authors formulate a HIBS-enabled cell switching framework as a mixed-integer programming (MIP) problem and evaluate it under realistic 3GPP channel models. The results indicate that energy savings for the HIBS-assisted cell switching approach are significantly better than traditional terrestrial approaches while maintaining high levels of served traffic.

The author in [35] focuses on improving both energy efficiency and latency performance in future 6G cellular networks through cell switching. The proposed approach improves energy efficiency by switching off idle or lightly loaded BSs and reducing the number of handovers, which contribute significantly to latency. A MIP formulation has been developed and solved with a heuristic-based method. As a result, it is demonstrated that the presented architecture can reduce the energy consumption and the number of handovers. Thus, HIBS-assisted cell switching offers a promising approach for achieving sustainable and low-latency 6G networks.

Table 2.1 Detailed comparison of existing cell switching studies.

Ref.	Network	NTN/HIBS	Main Objective	Method	QoS/Latency	Propagation Awareness
[17]	TN	No	Green networking / energy efficiency	Review	Limited	No
[18]	TN	No	Energy and spectrum efficiency	Resource reallocation	QoS	No
[12]	TN/HetNet	No	Cell switching challenges	Survey/review	QoS-related	Limited
[19]	TN	No	Energy minimization	Sequential heuristic	Network performance	No
[20]	TN/HetNet	No	Traffic-aware energy saving	Analytical switching model	Coverage-oriented	No
[21]	TN	No	Energy saving with reliable coverage	Scheduling-aware switching	QoS/coverage	
[15]	TN	No	Energy-efficient switching	Reinforcement learning	QoS	No
[22]	TN	No	Energy-efficient 6G cell switching	FL + actor–critic RL	QoS	No
[8]	TN–NTN	Yes	Load balancing and energy efficiency	AI-driven resource allocation	General QoS	Limited
[23]	TN–UAV	UAV	Energy-efficient UAV-assisted switching	Analytical framework	QoS	Limited
[24]	TN–HIBS	HIBS	Traffic offloading and energy reduction	Offloading analysis	QoS	Limited
[25]	TN–HIBS	HIBS	Grid energy and cost reduction	Adaptive HIBS capacity allocation	QoS	Limited
[26]	TN–HIBS	HIBS	Sustainable RAN operation	HIBS support analysis	Limited	Limited
[27]	vHetNet	HIBS	Traffic-aware cell switching	Layer-aware switching	QoS	Limited
[28]	TN–HIBS	HIBS	Flexible switching under constraints	HIBS-assisted switching	QoS	Limited
[29]	TN–HIBS	HIBS	Energy saving with delay awareness	Lightweight Q-learning	Latency-aware	Limited
[30]	TN–HIBS	HIBS	Energy-efficient RAN design	Real-traffic simulation	Limited	Limited
[31]	vHetNet	HIBS	Cell load estimation	Q-learning	QoS-related	Limited
[32]	vHetNet	HIBS	Spatial-temporal traffic prediction	Prediction-based switching	QoS-related	Limited
[33]	vHetNet	HIBS	Load estimation and renewable-aware switching	Two-phase data-driven framework	QoS	Limited
[34]	vHetNet	HIBS	Sustainable HIBS-enabled switching	MIP formulation	Served traffic	3GPP channel model
[35]	TN–HIBS	HIBS	Energy and latency reduction	MIP + heuristic	Latency / handover	Limited

Despite these advances, existing studies still do not explicitly consider the controlled utilization of non-terrestrial resources, particularly HIBS, which may lead to excessive reliance on NTN infrastructure. This limitation highlights the need for a propagation- and rate-aware bounded-NTN cell switching framework, where HIBS usage is explicitly controlled through constraint-aware design rather than treated as an unlimited resource.

In general, existing studies demonstrate that HIBS can handle offloaded traffic and provide energy savings through cell switching. However, most of these works focus mainly on energy efficiency or traffic management and do not explicitly control the amount of traffic offloaded to HIBS. As a result, HIBS is often used as an unlimited offloading resource, which may increase reliance on non-terrestrial systems and negatively impact both user performance and energy consumption.

Consequently, the trade-off between energy efficiency and controlled non-terrestrial resource utilization remains largely unexplored in the context of HIBS-assisted cell switching. In particular, there is a lack of a systematic framework that incorporates non-terrestrial resource awareness into switching decisions. Therefore, the key challenge is to achieve energy-efficient cell switching while preventing excessive reliance on HIBS and maintaining acceptable levels of user connectivity, data rate performance, and fairness. This motivates the development of a bounded-NTN cell switching framework that explicitly limits HIBS utilization and preserves its role as a complementary support layer rather than a primary traffic carrier.

2.3 Research Gap Analysis

Although existing studies demonstrate the potential of HIBS-assisted cell switching to reduce network power consumption, most of them treat HIBS simply as an additional offloading layer without explicitly regulating its utilization. In such approaches, HIBS is often assumed to be continuously available to handle traffic from switched-off terrestrial BSs. However, excessive offloading to HIBS may change its role from a complementary support layer to a primary traffic carrier, negatively impacting both network efficiency and user experience.

Moreover, many existing energy-focused cell switching approaches primarily evaluate performance based on total network power consumption. However, realistic propagation conditions are not fully incorporated into the switching decision. In particular, factors such as BEL for indoor users and atmospheric attenuation in NTN links are often overlooked or considered separately. As a result, an energy-efficient solution may still degrade data rates, increase the number of unconnected users, reduce fairness, or lead to greater reliance on non-terrestrial resources.

To address these challenges, this thesis develops a propagation- and rate-aware bounded-NTN cell switching framework to balance energy efficiency, user-centric performance, and controlled NTN utilization in future TN–NTN systems.

CHAPTER 3

SYSTEM MODEL

3.1 Network Model

A network model consisting of one HIBS, one MBS, and multiple SBSs is considered. There are Γ SBSs indexed by $i \in \mathcal{S}$, where $\mathcal{S} = \{1, 2, \ldots, \Gamma\}$, as illustrated in Fig. 3.1. The MBS $\mathcal{M}$ and the HIBS $\mathcal{H}$ are placed at the center of the considered area, with the HIBS deployed at an altitude of 20 km, while the SBSs are uniformly distributed around them. The HIBS serves three primary functions in the network: (i) acts as a BS with wide-area coverage; (ii) support users offloaded from SBSs; and (iii) manage network traffic by utilizing its high capacity and strong line-of-sight (LoS) links [26]. The set of BSs is denoted by $\mathcal{B}$ and defined as $\mathcal{B} = \mathcal{S} \cup \mathcal{M} \cup \mathcal{H}$, where $\mathcal{S}$, $\mathcal{M}$, and $\mathcal{H}$ denote the sets of SBSs, the MBS, and HIBS, respectively.

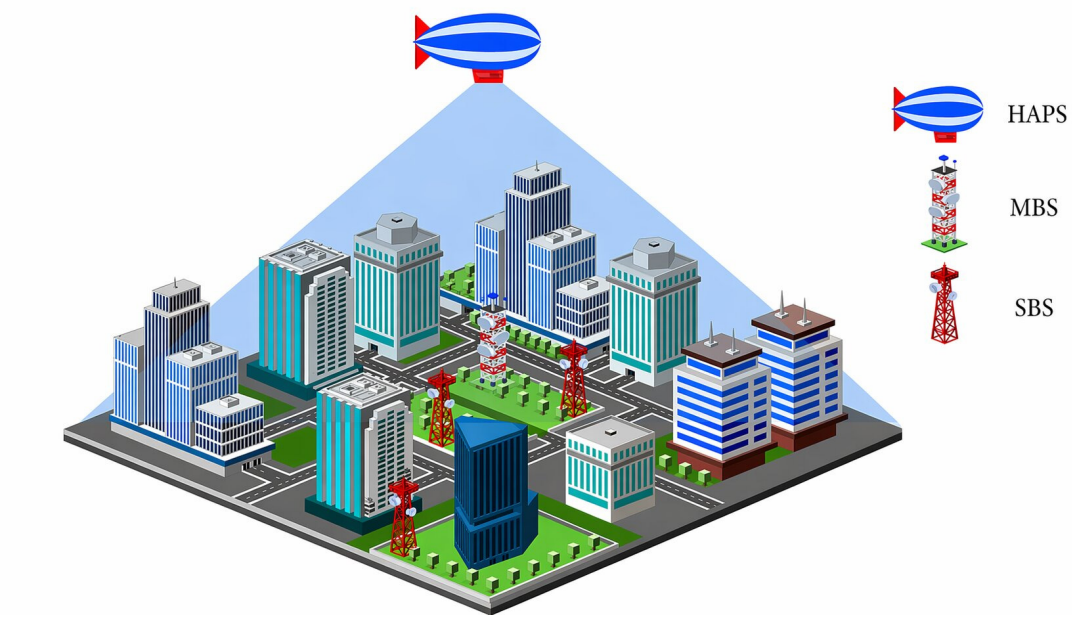


Figure 3.1 Multi-layer network model containing HIBS, MBS, SBSs.

UEs are initially uniformly distributed within the coverage area and move according to the random waypoint (RWP) mobility model. At each time slot, each UE may associate with any BS in $\mathcal{B}$ depending on channel conditions, coverage availability, and cell switching decisions. At any given time, each UE is associated with a single BS, and this association is adaptively updated in response to traffic conditions and cell switching

actions. SBS systems primarily serve nearby users, providing more localized coverage, whereas the MBS offers broader baseline coverage across the service area. The HIBS complements the terrestrial infrastructure by offering additional coverage and capacity, particularly when SBSs are switched off or experience congestion [26]. As a result, this heterogeneous architecture enables flexible traffic redistribution across network layers and provides the cell switching and optimization framework developed in this work.

Let $b \in \mathcal{B}$ denote the index of a BS. The network also consists of χ UEs, indexed by $u \in \mathcal{U}$, where $\mathcal{U} = \{1, 2, \ldots, \chi\}$.The UEs are uniformly distributed over a square area of size $\mathcal{A} \times \mathcal{A}$, where the position of each UE u is given by $\mathbf{x}_u = (x_u, y_u)$ with $x_u, y_u \sim \mathcal{U}(0, \mathcal{A})$ and $\mathcal{A} = 1$ km. The total number of users $\mathcal{U}$ is partitioned equally among high-loss, low-loss, and outdoor users. These user types are defined as follows:

- High-loss indoor users: UEs located indoors and experiencing severe BEL. This is modeled by assigning a high BEL, e.g., BEL $\approx 26\,$dB, representing users located in the interior of buildings, as shown in Table 3.1.
- Low-loss indoor users: UEs located indoors but closer to windows or building edges, experiencing moderate BEL. This is modeled with a lower BEL, e.g., BEL $\approx 15\,$dB, as demonstrated in Table 3.1.
- Outdoor users: UEs located in open environments without BEL, i.e., BEL $= 0,$dB.

This classification enables the model to reflect differences in signal attenuation caused by building penetration and surrounding materials. Each user category is therefore characterized by distinct propagation conditions, which directly affect the received signal strength and overall link quality. Consequently, user association and cell switching decisions are affected not only by traffic load but also by environment-dependent channel conditions.

3.2 Mobility Model

User mobility is modeled according to the RWP model, in which users are initially placed at random locations and then move toward uniformly distributed waypoints

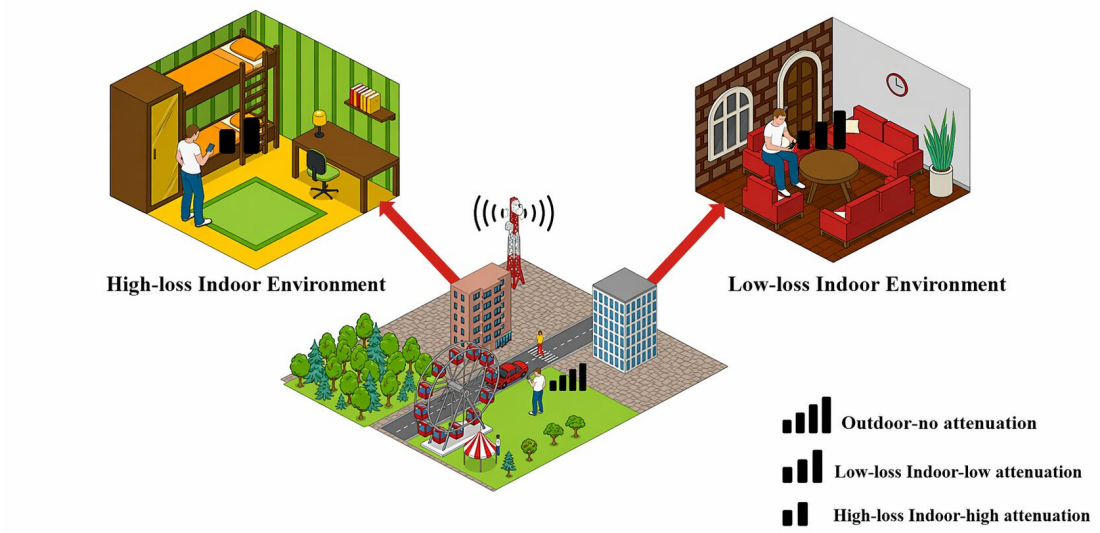


Figure 3.2 High-loss, low-loss indoor and outdoor users.

within the deployment area. Each user travels toward the selected waypoint with a randomly chosen speed drawn from a predefined range. Upon reaching the destination, a new waypoint and movement speed are randomly selected, after which the process repeats. This mobility model captures the dynamic nature of user movement over time, leading to realistic spatial traffic variations and allowing the assessment of cell switching and user association behavior under changing network conditions. Initially, each user is assigned a starting waypoint that is uniformly distributed over the considered deployment area. This initialization is mathematically expressed as

$$\mathbf{w}_u(0) \sim \mathcal{U}(\mathcal{A}), \tag{3.1}$$

where $\mathbf{w}_u(0)$ and $\mathcal{U}(\mathcal{A})$ denote the initial waypoint of user u a time $t = 0$ and the uniform distribution over the area $\mathcal{A}$, respectively. After selecting the initial waypoint, each user is assigned a movement speed drawn from a uniform distribution over a predefined interval to capture heterogeneous mobility behavior, as follows

$$v_u \sim \mathcal{U}(v_{\min}, v_{\max}), \tag{3.2}$$

where $v_{\min}$ and $v_{\max}$ represent the minimum and maximum user speeds, respectively. Given the selected waypoint and movement speed, the position of each user is updated

over time by moving in the direction of the current waypoint. The position update at each time step Δt is given by

$$\mathbf{x}_u(t+\Delta t) = \mathbf{x}_u(t) + v_u \Delta t \frac{\mathbf{w}_u(t) - \mathbf{x}_u(t)}{\|\mathbf{w}_u(t) - \mathbf{x}_u(t)\|}, \tag{3.3}$$

where $\mathbf{x}_u(t)$, $\mathbf{w}_u(t)$, and v_u denote the position of user u, the randomly selected waypoint, and the randomly selected speed, respectively. The movement toward a waypoint continues until the user reaches a sufficiently close range of the target location. This condition is defined as

$$\left\|\mathbf{w}_u(t) - \mathbf{x}_u(t)\right\| \leq \varepsilon, \tag{3.4}$$

where $\varepsilon > 0$ is a predefined proximity threshold. Once this condition is satisfied, a new waypoint is selected uniformly at random from the deployment area $\mathcal{A}$, and the movement process repeats.

3.3 Propagation Model

Given the presence of both TN and NTN in the considered network, path loss is modeled separately for each. This distinction is necessary because TN and NTN links are characterized by fundamentally different propagation environments and channel characteristics. Terrestrial links are primarily affected by factors such as distance-dependent attenuation, BEL and shadowing caused by surrounding obstacles. In contrast, NTN links, particularly with HIBS, usually have strong LoS conditions but are affected by altitude, large-scale path geometry, and atmospheric attenuation. Therefore, separate path loss models are used to realistically capture the propagation behavior of TN and NTN links and to ensure accurate evaluation of cell switching and user association decisions across network layers.

3.3.1 Path Loss Model for TN

The path loss between a TN BS and a UE is modeled using the 3rd Generation Partnership Project (3GPP) Urban Macro (UMa) model [36], which accounts for both LoS and non-LoS (NLoS) propagation conditions. This model is chosen because it is widely used in the literature and provides a realistic representation of large-scale

propagation effects in dense urban environments, where buildings and surrounding structures significantly influence signal attenuation. In particular, the UMa model incorporates distance-dependent path loss and probabilistic LoS occurrence. Accordingly, the LoS path loss for TN links is computed as

$$L_{\mathrm{LoS}} = 28 + 22\log_{10}(d_{\mathrm{3D}}) + 20\log_{10}(f_{\mathrm{GHz}}) + \sigma_{\mathrm{LoS}} + L_{\mathrm{BEL}}, \tag{3.5}$$

where d_{3D} represents the three-dimensional distance between the BS and UE, and f_{GHz}, σ_{LoS}, and L_{BEL} represent the carrier frequency, shadowing, and BEL, respectively. In a similar vein, the path loss for NLoS TN is evaluated by

$$L_{\mathrm{NLoS}} = 32.54 + 30\log_{10}(d_{\mathrm{3D}}) + 20\log_{10}(f_{\mathrm{GHz}}) + \sigma_{\mathrm{NLoS}} + L_{\mathrm{BEL}}. \tag{3.6}$$

Following the 3GPP UMa model in [36], the LoS probability is formulated as a function of the horizontal distance between the BS and the UE. This probabilistic representation reflects the strong dependence of LoS conditions in urban environments on user location, building density, and the surrounding physical environment. As the distance increases, the probability of maintaining an unobstructed propagation path generally decreases due to the growing impact of buildings and urban clutter. Accordingly, the LoS probability is modeled to capture this distance-dependent behavior and is expressed as

$$\Pr_{\mathrm{LoS}} = \begin{cases} 1, & d_{\mathrm{2D\text{-}out}} \le 18 \text{ m}, \\ \left[\min\left(\dfrac{18}{d_{\mathrm{2D\text{-}out}}}, 1\right)\left(1 - \exp\left(-\dfrac{d_{\mathrm{2D\text{-}out}}}{63}\right)\right) \right. & \\ \left. \quad + \exp\left(-\dfrac{d_{\mathrm{2D\text{-}out}}}{63}\right)\right](1 + C'(h_{\mathrm{UT}})), & d_{\mathrm{2D\text{-}out}} > 18 \text{ m}, \end{cases} \tag{3.7}$$

where $\Pr_{\mathrm{LoS}}$ and $d_{\mathrm{2D\text{-}out}}$ denote the probability that a LoS propagation condition exists between the BS and the UE and the horizontal (two-dimensional) distance between BS and UE in the outdoor environment, respectively.

$$C'(h_{\mathrm{UT}}) = \begin{cases} 0, & h_{\mathrm{UT}} \le 13 \text{ m}, \\ \left(\dfrac{h_{\mathrm{UT}} - 13}{10}\right)^{1.5}, & 13 < h_{\mathrm{UT}} \le 23 \text{ m}, \end{cases} \tag{3.8}$$

where $C'(h_{\mathrm{UT}})$ and h_{UT} represent the height-dependent correction factor that accounts for the impact of UE elevation on the LoS probability and the height of the UE above ground level, respectively.

L_{BEL} is expressed as the sum of a baseline BEL, expressed as

$$L_{\mathrm{BEL}} = L_{\mathrm{BEL,base}} + L_{\mathrm{E}}, \tag{3.9}$$

where $L_{\mathrm{BEL,base}}$ and L_{E} denote the baseline BEL and the additional loss term, respectively. L_{E} is defined as

$$L_{\mathrm{E}} = \begin{cases} 26, & \text{High-loss indoor [2].} \\ 15, & \text{Low-loss indoor [2].} \\ 0, & \text{Outdoor,} \end{cases} \tag{3.10}$$

where L_{E} is introduced to distinguish different propagation environments and user type. In particular, high-loss indoor users experience extra attenuation beyond the baseline BEL, whereas low-loss indoor users encounter a smaller attenuation.

Table 3.1 BEL values for traditional and modern office buildings at different frequencies [2].

Frequency	Traditional Office Building		Modern Office Building	
	Mean	STD	Mean	STD
800 MHz	14.3	5.4	21.8	5.4
2 GHz	14.7	7.1	25.9	5.9
3.5 GHz	17.8	7.4	28.9	6.3
5.2 GHz	17.7	6.0	37.0	6.9
10 GHz	22.3	7.9	39.1	6.5
18 GHz	21.9	8.9	49.9	6.8
28 GHz	26.4	9.5	39.0*	3.9*

As illustrated in Table 3.1, additional losses are determined based on traditional and modern office building assumptions at 2 GHz, representing low-loss and high-loss indoor environments, respectively. Outdoor users, on the other hand, are not affected by BEL.

3.3.2 Path Loss Model for NTN

The HIBS path loss model follows the 3GPP report in [36]. As the signal propagates between the HIBS and the UE, it experiences several sources of attenuation associated with large-scale propagation. In particular, signal degradation increases with distance and is further influenced by atmospheric effects and the surrounding user environment. As a result, the overall path loss, denoted by L_{HIBS}, reflects the combined effect of these factors and is given by

$$L_{\text{HIBS}} = L_{\text{FSPL}} + L_{\text{a}} + L_{\text{BEL}}, \tag{3.11}$$

where L_{FSPL} and L_{a} are the free space path loss (FSPL) and attenuation caused by atmospheric losses, respectively. L_a is computed by

$$L_{\text{a}} = \left(A_{\text{gas}} + A_{\text{rain}}\right) \cdot d_{\text{slant}}, \tag{3.12}$$

where A_{rain} and A_{gas} denote the specific attenuations (dB/km) due to rain and atmospheric gases, respectively, and d_{slant} is the slant distance (km). In this work, gas and rain attenuations are obtained from ITU-R P.676 [37], expressed as

$$A_{\text{rain}} = \gamma_R = kr^{\alpha}, \tag{3.13}$$

where k and α depend on frequency and polarization, and r is the rain rate (mm/h) exceeded for 0.01% of an average year. For our simulations, the carrier frequency is $f = 2\,\text{GHz}$ and the rain attenuation statistics are evaluated for 0.01% time. Finally, d_{slant} is the slant distance, which is calculated by

$$d_{\text{slant}} = \sqrt{R_E^2 \sin^2(\theta) + h_{\text{HIBS}}^2 + 2h_{\text{HIBS}}R_E} - R_E \sin(\theta), \tag{3.14}$$

where R_E, θ, and h_{HIBS} represent the Earth's radius, the elevation angle, and the HIBS altitude, respectively.

3.4 Power Consumption Model

This thesis employs the EARTH power model presented in [38] to determine the instantaneous power consumption of each BS. Hence, the power consumption $P_{b,t}$, of BS b at time t is calculated as

$$P_{b,t} = \begin{cases} P_{\mathrm{O},b} + \eta_b \lambda_{b,t} P_{\mathrm{T},b}, & 0 < \lambda_{b,t} < 1, \\ P_{\mathrm{S},b}, & \lambda_{b,t} = 0, \end{cases} \tag{3.15}$$

where $P_{\mathrm{T},b}$ is the BS transmit power, $P_{\mathrm{O},b}$ is the operational circuit power, η_b is the efficiency, $P_{\mathrm{S},b}$ is the sleep circuit power, $\lambda_{b,t}$ is the instantaneous load factor at time t, and computed as

$$\lambda_{b,t} = \frac{\zeta_{b,t}}{\zeta_{\mathrm{T}}}, \tag{3.16}$$

where $\zeta_{b,t}$ corresponds to the number of resource blocks (RBs) used in BS b at time t, and ζ_{T} is the total number of RBs available in the BS. In addition, a fixed bandwidth of 200 kHz is allocated to each user. The value of ζ_{T} is determined by dividing the total bandwidth of the BS by 200 kHz. The total instantaneous network power consumption, P, at time t is calculated

$$P_t = P_{\mathrm{H}} + P_{\mathrm{M}} + \sum_{i \in \mathcal{S}} P_{i,t}, \tag{3.17}$$

where P_H, P_M, and s denote the power consumption of the HIBS, the power consumption of the MBS, and the number of SBSs deployed in the network, respectively.

Table 3.2 Power parameters of various BS types.

BS Type	**Efficiency** η_b	**Transmit** $P_{\mathrm{T},b}$ **[W]**	**Operational** $P_{\mathrm{O},b}$ **[W]**	**Sleep** $P_{\mathrm{S},b}$ **[W]**
HIBS	4.7	20	130	75
MBS [38]	4.7	20	130	75
SBS [38]	2.6	6.3	56	39

Table. 3.2 illustrates the power-related parameters of different BS types considered in

this thesis. Specifically, the table shows the power amplifier efficiency, transmit power, operational power consumption, and sleep-mode power for HIBS, MBS, and SBS. These parameters are used to model the energy consumption characteristics of each BS type.

3.5 User Allocation

User allocation is performed according to the signal-to-interference-plus-noise ratio (SINR) received by each user from each BS. This quantity characterizes the joint effect of the desired signal power, interference from neighboring BSs, and thermal noise on the received link quality. Accordingly, the SINR of user u from BS b is expressed as

$$\gamma_{u,b} = \frac{P_{u,b}}{P_{\mathrm{n}} + \sum\limits_{k \in \mathcal{B}_{\mathrm{act}} \setminus \{b\}} P_{u,k}}, \tag{3.18}$$

where $P_{u,b}$, P_{n}, and $P_{u,k}$ denote the received power from BS b, the noise power, and interference power, respectively.

To associate users with a BS, following conditions must be satisfied:

i) The selected BS should offer the maximum SINR compared to the other BSs, such that

$$b_u^{\star} = \arg\max_{b \in \mathcal{B}} \ \gamma_{u,b}, \tag{3.19}$$

where $b_u^{\star}$ denotes the serving BS for user u.

ii) The BS must have a sufficient number of available RBs to accommodate the user

$$\zeta_b^{\mathrm{used}} + \zeta_{\text{per-user}} \leq \zeta_b^{\mathrm{T}}, \tag{3.20}$$

where ζ_b^{used}, $\zeta_{\text{per-user}}$, and ζ_b^{T} represent the number of used RBs, the RBs per user, and the total RBs of the BSs, respectively.

iii) The user's received signal power must be higher than the receiver reference

sensitivity, such that

$$\iota_{u,b} \geq \iota_{\text{ref}}, \quad \forall u \in \mathcal{U}, \forall b \in \mathcal{B}, \tag{3.21}$$

where $\iota_{u,b}$ and ι_{ref} denote the received signal strength from BS b to user u, and the receiver reference sensitivity, respectively. The received signal strength $\iota_{u,b}$ is expressed as

$$\iota_{u,b} = \begin{cases} P_{\text{T},b} - L_{\text{LoS}}, & \text{TN (LoS)}, \\ P_{\text{T},b} - L_{\text{NLoS}}, & \text{TN (NLoS)}, \\ P_{\text{T},b} - L_{\text{HIBS}}, & \text{NTN (HIBS)}. \end{cases} \tag{3.22}$$

As shown in Equation **3.22**, the received signal strength at user u from BS b depends on the propagation scenario. In this context, the received signal strength is obtained by subtracting the corresponding path loss from the BS transmit power. This formulation provides a consistent representation of the received signal level while allowing the appropriate path loss model to be applied based on the underlying propagation condition.

CHAPTER 4

PROBLEM FORMULATION

This chapter introduces the SBS switching and power-level configuration as an optimization problem aimed at minimizing the total network power consumption under load and sensitivity constraints, while simultaneously limiting the number of unconnected users. The state vectors $\Delta = [\delta_{1,t}, \delta_{2,t}, \ldots, \delta_{\Gamma,t}]^\intercal$ and $\Omega = [\rho_{1,t}, \rho_{2,t}, \ldots, \rho_{\Gamma,t}]^\intercal$ represent the ON/OFF states and the power-level of SBSs, respectively. Based on these control variables, the network power consumption is jointly determined by the active SBSs set and their corresponding transmission configurations. In contrast, the MBS and HIBS are assumed to be continuously operational and to operate at full transmit power, and hence are excluded from the ON/OFF switching decision space [27, 29]. To move beyond a solely energy-focused formulation, a constrained multi-objective optimization model based on the ϵCM is developed from the EFM. The proposed model extends the baseline formulation by jointly considering energy efficiency, user connectivity, and controlled utilization of HIBS.

4.1 Conventional Energy-Focused Cell Switching Problem Formulation (EFM)

The cell switching problem is commonly formulated as an optimization task that seeks to minimize the total network power consumption by dynamically controlling the states of BSs [27, 28], i.e.,

$$\min_{\Delta} \quad P(\Delta) \tag{4.1}$$

$$\text{s.t.} \quad \lambda_{\mathrm{H},t} \leq 1, \tag{4.1a}$$

$$\lambda_{\mathrm{M},t} \leq 1, \tag{4.1b}$$

$$\delta_{i,t} \in \{0, 1\}, \quad i = 1, \ldots, \Gamma. \tag{4.1c}$$

where $\delta_{i,t} = 0$ and $\delta_{i,t} = 1$ represent the OFF and ON state of the BSs, respectively. Also, $\lambda_{\mathrm{H},t}$ and $\lambda_{\mathrm{M},t}$ denote the load factors of the HIBS and MBS, respectively. The total network power consumption is defined as

$$P(\Delta) = (P_{\mathrm{O,H}} + \eta_{\mathrm{H}}\lambda_{\mathrm{H,t}}P_{\mathrm{T,H}}) + (P_{\mathrm{O,M}} + \eta_{\mathrm{M}}\lambda_{\mathrm{M,t}}P_{\mathrm{T,M}}) + \sum_{i\in\mathcal{S}}\Big[(P_{\mathrm{O},i} + \eta_i\lambda_{i,t}P_{\mathrm{T},i})\,\delta_{i,t} + P_{S,i}(1-\delta_{i,t})\Big]. \tag{4.2}$$

The total network power consumption is formulated to reflect the combined energy expenditure of a heterogeneous network composed of always-on infrastructure elements and dynamically switchable SBSs. In this model, the MBS and the HIBS contribute a baseline power consumption that is independent of switching decisions, while their traffic-dependent power components scale with the instantaneous network load. In contrast, the power consumption of SBSs is controlled through the switching vector Δ, allowing binary ON/OFF switching. As a result, the model captures the fundamental trade-off between maintaining user connectivity and reducing energy consumption by selectively activating SBSs only when required by traffic demand. By incorporating fixed operational costs, load-dependent transmission power, and sleep-mode savings, the proposed model provides a practical basis for energy-efficient optimization in heterogeneous TN-NTN.

To extend the conventional ON/OFF cell switching model, an additional power-level state vector Ω is considered to enable transmit-power adaptation for active SBSs, expressed as

$$\Omega = [\rho_{1,t}, \rho_{2,t}, \ldots, \rho_{\Gamma,t}]^{\mathsf{T}}, \tag{4.3}$$

where Ω represents the power-level state vector collecting the $\rho_{i,t}$ variables of all SBSs at time t, defined as

$$\rho_{i,t} \in \{0, 1\}, \quad i = 1, \ldots, \Gamma, \tag{4.4}$$

where $\rho_{i,t}$ is a discrete power-level state variable for SBS i at time t, with $\rho_{i,t} = 0$

corresponding to 20% transmit power, $\rho_{i,t} = 1$ to full (100%) transmit power. To express these levels compactly, define the power scaling factor

$$\phi(\rho_{i,t}) = \begin{cases} 0.2, & \rho_{i,t} = 0, \\ 1, & \rho_{i,t} = 1. \end{cases} \tag{4.5}$$

For BS i, the power model induced by $(\delta_{i,t}, \rho_{i,t})$ can be written as

$$P_{i,t}(\delta_{i,t}, \rho_{i,t}) = \begin{cases} P_{\mathrm{S},i}, & \delta_{i,t} = 0, \\ P_{\mathrm{O},i} + \eta_i \lambda_{i,t} P_{\mathrm{T},i}\, \phi(\rho_{i,t}), & \delta_{i,t} = 1. \end{cases} \tag{4.6}$$

The power consumption model for SBSs is formulated to jointly capture binary ON/OFF decisions and transmit power-level selection within a unified framework. Specifically, the model considers two states: an OFF state, where the SBS is in sleep mode, and an ON state, where power consumption increases based on the transmit power level and traffic load. The formulation integrates the ON/OFF switching variable with the power-level decision, allowing SBS operation to adapt to traffic conditions while minimizing unnecessary energy consumption. This joint modeling approach enables the optimization framework to leverage both switching and power control decision variables, thereby achieving improved energy efficiency without compromising network operability. Accordingly, the effective transmit power of SBS i at time t, which jointly reflects the ON–OFF switching decision and the selected power level, is defined as in Equation **4.7**, while the practical implications of this formulation are conceptually illustrated in Fig. 4.1. The effective transmit power is mathematically defined as

$$\kappa_{i,t} = P_{\mathrm{T},i} \delta_{i,t}\, \phi(\rho_{i,t}), \quad i = 1, \ldots, \Gamma, \tag{4.7}$$

where $\kappa_{i,t}$ is not an independent decision variable but is determined by its ON/OFF and power-level states. If the BS is OFF ($\delta_{i,t} = 0$), then $\kappa_{i,t} = 0$. Otherwise, when the SBS is ON ($\delta_{i,t} = 1$), $\kappa_{i,t}$ is scaled according to the selected power level $\rho_{i,t}$. This formulation avoids introducing additional decision variables while preserving the coupling between switching and power-level selection. Consequently, the total network

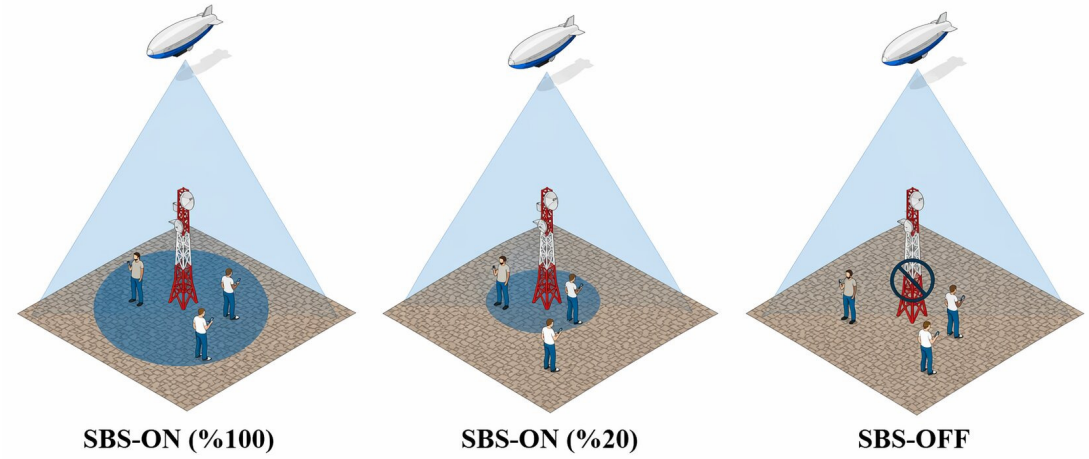


Figure 4.1 Illustration of SBS operating modes and their impact on coverage and HIBS offloading.

power consumption in terms of Δ and Ω can be compactly expressed as

$$P(\Delta,\Omega) = \left(P_{\mathrm{O,H}} + \eta_{\mathrm{H}}\lambda_{\mathrm{H},t}P_{\mathrm{T,H}}\right) + \left(P_{\mathrm{O,M}} + \eta_{\mathrm{M}}\lambda_{\mathrm{M},t}P_{\mathrm{T,M}}\right) + \sum_{i\in\mathcal{S}}\left[P_{\mathrm{O},i}\,\delta_{i,t} + \eta_i\lambda_{i,t}\kappa_{i,t} + P_{\mathrm{S},i}(1-\delta_{i,t})\right]. \tag{4.8}$$

Then, the conventional energy-focused formulation can be expressed using the state vector Ω denoted as

$$\min_{\Delta,\Omega} \quad P(\Delta,\Omega) \tag{4.9}$$

s.t. **(4.1a) – (4.1c)**,

(4.4),

(4.7).

The formulation minimizes the total network power consumption by jointly optimizing the SBS ON/OFF states and their transmit power levels.

This joint modeling is adopted because ON/OFF switching and transmit-power scaling capture two complementary energy-saving modes that are both relevant in practice. In particular, the binary variable $\delta_{i,t} \in \{0,1\}$ represents the deep-sleep decision (i.e., completely switching an SBS off and only consuming $P_{\mathrm{S},i}$), which

typically provides substantial energy savings but may force user offloading. Meanwhile, the discrete power-scaling variable $\rho_{i,t} \in \{0, 1\}$ represents operating an active SBS at different transmit-power levels through $\kappa_{i,t} = P_{\mathrm{T},i}\,\delta_{i,t}\,\phi(\rho_{i,t})$ as defined in Equation **4.7**. Hence, $\rho_{i,t} = 0$ enables low-power operation to reduce both transmitted power and interference, while $\rho_{i,t} = 1$ allows full-power transmission when required by traffic demand and QoS constraints. Overall, combining ON/OFF switching with power-level scaling provides a more flexible energy–QoS trade-off than using only ON/OFF decisions.

Three operating states are considered:

- ON: The HIBS, the MBS, and SBS i are all active.
- OFF: The HIBS and the MBS remain active while SBS i is switched OFF. The traffic originally served by SBS i is offloaded to the network.
- PS (Power Scaling): SBS i remains active but applies transmit-power scaling according to the selected level ρ (e.g., 20%). This may also induce additional load on the MBS due to traffic redistribution.

Due to the identical power consumption parameters of the MBS and HIBS, the offloading impact is analyzed using a representative MBS-based scenario to simplify the analysis. Let $\Delta\lambda^{(i)}_{\mathrm{M},t} \geq 0$ denote the incremental MBS load due to switching SBS i OFF. Then, the resulting network-wide power saving (ON → OFF) is

$$\Delta P^{\mathrm{ON}\leftarrow\mathrm{OFF}}(i) \triangleq P_{\mathrm{ON}} - P_{\mathrm{OFF}} = \left(P_{\mathrm{O},i} + \eta_i \lambda_{i,t} P_{\mathrm{T},i}\right) - P_{\mathrm{S},i} - \eta_{\mathrm{M}}\, P_{\mathrm{T,M}}\, \Delta\lambda^{(i)}_{\mathrm{M},t}. \tag{4.10}$$

Here, $\Delta P^{ON\leftarrow OFF}$ defined as the difference between the corresponding total network power consumptions. Hence, switching SBS i OFF reduces the total network power if $\Delta P^{\mathrm{ON}\leftarrow\mathrm{OFF}}(i) > 0$, i.e., when the local SBS saving dominates the additional MBS power induced by offloading.

To relate $\Delta\lambda^{(i)}_{\mathrm{M},t}$ to the RBs offloaded to the MBS, let $\Delta\zeta^{(i)}_{\mathrm{M},t}$ and $\Delta\zeta^{(i,\rho)}_{\mathrm{M},t}$ denote the

additional number of RBs scheduled by the MBS when SBS i is switched OFF or power-scaled at level ρ, respectively. Since the MBS load factor is defined as the fraction of utilized RBs, the load increments can be written as

$$\Delta\lambda_{\mathrm{M},t}^{(i)} = \frac{\Delta\zeta_{\mathrm{M},t}^{(i)}}{\zeta_{\mathrm{M}}^{\mathrm{tot}}}, \qquad \Delta\lambda_{\mathrm{M},t}^{(i,\rho)} = \frac{\Delta\zeta_{\mathrm{M},t}^{(i,\rho)}}{\zeta_{\mathrm{M}}^{\mathrm{tot}}}. \tag{4.11}$$

Moreover, $\Delta\zeta_{\mathrm{M},t}^{(\cdot)}$ can be approximated as the number of users offloaded to the MBS multiplied by the RB demand per user defined in Equation **3.16**.

The power saving obtained by keeping SBS i ON but applying power scaling with $\rho = 0$ corresponding to 20% of relative to the baseline is expressed as

$$\begin{aligned} \Delta P^{\mathrm{ON}\leftarrow\mathrm{PS}}(i,\rho) &\triangleq P_{\mathrm{ON}} - P_{\mathrm{PS}} \\ &= \eta_i \lambda_{i,t} P_{\mathrm{T},i}(1-\phi(\rho)) - \eta_{\mathrm{M}} P_{\mathrm{T,M}} \Delta\lambda_{\mathrm{M},t}^{(i,\rho)}. \end{aligned} \tag{4.12}$$

For the two power-scaled operating points, this becomes

$$\Delta P^{\mathrm{ON}\leftarrow\mathrm{PS}}(i,0) = 0.8\,\eta_i \lambda_{i,t} P_{\mathrm{T},i} - \eta_{\mathrm{M}} P_{\mathrm{T,M}} \Delta\lambda_{\mathrm{M},t}^{(i,0)}. \tag{4.13}$$

Accordingly, under high-load conditions where switching SBS i OFF would induce a large increment in MBS load, applying 20% power scaling while keeping the SBS ON can be more energy-efficient than switching the SBS OFF. This holds when the network-wide saving obtained by 20% power scaling exceeds the saving obtained by switching OFF, i.e.,

$$\Delta P^{\mathrm{ON}\leftarrow\mathrm{PS}}(i,0) > \Delta P^{\mathrm{ON}\leftarrow\mathrm{OFF}}(i). \tag{4.14}$$

Using Equation **4.10** and the 20% case above, the condition can be written explicitly as

$$0.8\,\eta_i \lambda_{i,t} P_{\mathrm{T},i} - \eta_{\mathrm{M}} P_{\mathrm{T,M}} \Delta\lambda_{\mathrm{M},t}^{(i,0)} > \left(P_{\mathrm{O},i} + \eta_i \lambda_{i,t} P_{\mathrm{T},i}\right) - P_{\mathrm{S},i} - \eta_{\mathrm{M}} P_{\mathrm{T,M}} \Delta\lambda_{\mathrm{M},t}^{(i)}. \tag{4.15}$$

In particular, if the OFF decision leads to a much larger MBS-load increment than 20% power scaling (i.e., $\Delta\lambda_{\mathrm{M},t}^{(i)} \gg \Delta\lambda_{\mathrm{M},t}^{(i,0)}$), then the OFF-induced MBS power term dominates

and 20% power scaling becomes preferable.

4.2 Multi-Objective Optimization Problem Formulation

The EFM in Equation **4.9** focuses on minimizing the total network power consumption; however, it does not explicitly control the reliance on NTN resources or account for potential user performance degradation after cell switching. In HIBS-assisted architectures, switching off terrestrial BSs may unintentionally shift a significant portion of the traffic to the HIBS-SMBS. Although HIBS provides extended coverage and additional capacity, excessive reliance on this NTN platform may increase its load and potentially reduce the intended energy-efficiency gains of terrestrial cell switching. Therefore, beyond the energy minimization objective, additional performance metrics are introduced. First, the utilization of the HIBS platform is explicitly modeled in order to prevent excessive reliance on NTN resources. Subsequently, user-centric performance indicators, such as the number of unconnected and dissatisfied users after cell switching, as well as fairness across users, are incorporated to ensure that energy-efficient operation does not compromise connectivity and service quality.

One of the key objectives is to limit the reliance on NTN resources by minimizing the utilization of the HIBS after cell switching. In integrated TN–NTN frameworks, uncontrolled traffic offloading may shift the traffic load to HIBS, thereby turning it into a primary traffic carrier rather than a complementary support platform. The metric $H(\Delta, \Omega)$ represents the number of users associated with the HIBS after cell switching and therefore captures the extent to which traffic is redirected to the NTN segment. By minimizing this metric, the proposed framework specifically limits the utilization of HIBS resources, ensuring that the NTN platform operates as a complementary component of the network rather than an unlimited traffic absorber. This formulation allows HIBS to support the network when necessary, while preventing it from becoming

the dominant traffic carrier, such that

$$\begin{aligned} \min_{\Delta,\Omega} \quad & H(\Delta,\Omega) \\ \text{s.t.} \quad & \textbf{(4.1a) – (4.1c)}, \\ & \textbf{(4.4)}, \\ & \textbf{(4.7)}. \end{aligned} \tag{4.16}$$

where H is the HIBS usage under cell switching and BS ON/OFF pattern. In addition, the HIBS usage counter is denoted as

$$H = \sum_{u\in\mathcal{U}} \sum_{b\in\mathcal{H}} s^a_{u,b}, \tag{4.17}$$

where $\mathcal{B}_H$ and $s^a_{u,b}$ denote the set of HIBS and binary association indicator that shows whether user u is associated to HIBS, defined as

$$s^a_{u,b} = \begin{cases} 1, & \text{if user } u \text{ is associated with HIBS,} \\ 0, & \text{otherwise.} \end{cases} \tag{4.18}$$

The binary variable $s^a_{u,b}$ indicates whether user u is associated with the HIBS after cell switching. It takes the value 1 if user u is served by the HIBS and 0 otherwise. Through this indicator, the proposed formulation identifies users offloaded to the NTN platform after switching.

Although limiting the utilization of the HIBS prevents excessive reliance on NTN resources, the proposed framework does not eliminate HIBS usage entirely, but rather bounds it within an acceptable level. Nevertheless, cell switching may also affect the connectivity of users within the network. In particular, switching off certain BSs may lead to situations where some users cannot be associated with any available BS due to insufficient received signal strength or resource availability. Therefore, in addition to limiting HIBS utilization, it is necessary to consider user connectivity within the optimization framework. To account for this effect, an additional objective is introduced to minimize the number of unconnected users during the cell switching

process. Accordingly, the number of unconnected users is mathematically defined as follows

$$\min_{\Delta,\Omega} \quad U(\Delta,\Omega) \tag{4.19}$$

s.t. **(3.21)**,

(4.1a) – (4.1c),

(4.4),

(4.7).

The feasibility indicator $f_{u,b}$ allows user association only with active BSs that satisfy both the receiver sensitivity requirement and the RB availability constraint. In this way, BSs that cannot provide a detectable signal or lack sufficient radio resources are excluded from the candidate set for user association. This process ensures that only feasible communication links are considered during the association process. Once the set of feasible BSs is identified, the user u associates with the BS that provides the highest SINR among these candidates, in accordance with Equation **3.19**. This selection strategy reflects a common association policy in cellular systems, where users prioritize the link that provides the strongest signal quality while respecting resource availability constraints. The feasibility indicator is given by

$$f_{u,b} = \begin{cases} \delta_{b,t}\, \mathbb{1}\{\iota_{u,b} \geq \iota_{\text{ref}}\}\, \mathbb{1}\{\zeta_b^{\text{used}} + \zeta^{\text{per}} \leq \zeta_b^{\text{tot}}\}, & b \in \mathcal{S}, \\ \mathbb{1}\{\iota_{u,b} \geq \iota_{\text{ref}}\}\, \mathbb{1}\{\zeta_b^{\text{used}} + \zeta^{\text{per}} \leq \zeta_b^{\text{tot}}\}, & b \in \{\mathcal{M}, \mathcal{H}\}. \end{cases} \tag{4.20}$$

If $f_{u,b} = 0$ for all b, user u is considered unconnected, as there is no feasible association that simultaneously satisfies the receiver sensitivity and RB availability conditions. In other words, the user cannot be served by any BS in the network under the current cell switching configuration. To capture this situation, a non-connection indicator z_u is introduced for each user, where $z_u = 1$ indicates that user u is connected, while $z_u = 0$ indicates that no feasible association is available. Consequently, the total number of unconnected users is obtained by summing these indicators over the entire user set, thereby capturing the impact of cell switching on service availability in the network.

Consequently, the number of unconnected users is calculated as

$$z_u = \mathbb{1}\left\{\sum_{b\in\mathcal{B}} f_{u,b} > 0\right\}. \tag{4.21}$$

The binary indicator z_u in Equation **4.21** identifies whether at least one feasible BS exists for user u. Based on this indicator, the total number of unconnected users in the network can be obtained by counting the users for which $z_u = 0$, which yields

$$U = \sum_{u\in\mathcal{U}} (1 - z_u). \tag{4.22}$$

Nevertheless, minimizing the number of unconnected users ensures that users remain associated with a BS after cell switching. However, connectivity alone does not guarantee acceptable service quality. Even when users remain connected, the reassociation to different BSs may lead to degraded SINR conditions and reduced achievable data rates due to increased propagation losses or higher interference levels. Consequently, some users may experience performance degradation despite maintaining connectivity. To address this effect, an additional optimization objective is introduced to minimize the number of dissatisfied users after cell switching. Accordingly, the number of dissatisfied users is defined as follows

$$\min_{\Delta,\Omega} \quad D(\Delta,\Omega) \tag{4.23}$$

s.t. **(3.21)**,

(4.1a) – (4.1c),

(4.4),

(4.7).

A dissatisfied user is defined as one whose achievable data rate after cell switching (R_u^{a}) becomes lower than the data rate obtained before cell switching (R_u^{b}). This situation may occur when a user is reassociated with a different BS that provides weaker received signal strength or experiences a higher path loss after the switching event. As a result, the SINR experienced by the user decreases, leading to a lower achievable data rate.

Such users are therefore regarded as dissatisfied, since the quality of service they receive declines compared to the pre-switching condition. Accordingly, this condition can be written as

$$R_u^{\mathrm{a}} < R_u^{\mathrm{b}}. \tag{4.24}$$

Initially, users connect to the BS that provides the maximum SINR. Following cell switching, this BS may be switched off for some users, causing some users to connect to farther BSs. This leads to a higher path loss and potentially lower received power, which may degrade both connectivity and post-switching service quality. The BS assignment challenge that emerges after cell switching can be expressed as

$$b_u^{(\mathrm{b})} \neq b_u^{(\mathrm{a})}, \qquad b_u^{(\mathrm{a})} \in \mathcal{B}_{\mathrm{act}}, \tag{4.25}$$

where $\mathcal{B}_{\mathrm{act}}$ denotes the set of active BSs, defined as

$$\mathcal{B}_{\mathrm{act}} = \{i \in \mathcal{S} \mid \delta_{i,t} = 1\} \cup \mathcal{M} \cup \mathcal{H}. \tag{4.26}$$

Here, $\mathcal{B}_{\mathrm{act}}$ includes all active SBSs as well as the always active MBS and HIBS. Therefore, after cell switching, a user may be reassociated to another active SBS, the MBS, or the HIBS. In addition, $b_u^{(\mathrm{b})}$ and $b_u^{(\mathrm{a})}$ denote the BSs serving user u before and after the cell switching operation, respectively. The condition $b_u^{(\mathrm{b})} \neq b_u^{(\mathrm{a})}$ indicates that the user is reassociated with a different BS after switching. In this case, the reassociation may introduce an additional propagation loss due to the change in the serving link. This effect is explicitly captured in the formulation as follows

$$\Delta L_u \triangleq L_{u,b}^{(\mathrm{a})} - L_{u,b}^{(\mathrm{b})} \geq 0. \tag{4.27}$$

To make Equation **4.27** more explicit using the propagation models adopted in Equation **3.5**, Equation **3.6** and Equation **3.11** we write the path loss of the

candidate links as

$$L_{u,b} = \begin{cases} L_{\mathrm{TN}}, & b \in \mathcal{S} \cup \mathcal{M}, \\ L_{\mathrm{HIBS}}, & b \in \mathcal{H}. \end{cases} \tag{4.28}$$

Then, the additional loss induced by reassociation becomes

$$\Delta L_u = L_{u,b}^{(\mathrm{a})} - L_{u,b}^{(\mathrm{b})}, \tag{4.29}$$

where the terms are evaluated according to the corresponding TN (LoS/NLoS) or NTN (HIBS) path-loss expressions above. In particular, if the post-switching association is to the HIBS, the NTN path loss in Equation **3.11** includes atmospheric attenuation and BEL, which can further increase $L_{u,b}^{(\mathrm{a})}$ relative to a terrestrial link.

An additional challenge after cell switching is the degradation of the received SINR, which in turn reduces the achievable data rate. Consequently, the increase in dissatisfied users leads to the problem stated in Equation **4.23**. A user is considered dissatisfied if the data rate after cell switching falls below the data rate before switching. The achievable rate of a user is defined by the Shannon capacity formula as

$$R_u = \mathrm{W} \log_2 (1 + \gamma_{u,b}). \tag{4.30}$$

Following cell switching, the user may be reassociated to a different BS, which typically increases the link distance and, consequently, the path loss. Using the additional path-loss term ΔL_u defined in Equation **4.27**, the received power is reduced, leading to a lower post-switching SINR, i.e.,

$$\gamma_u^{(\mathrm{a})} < \gamma_u^{(\mathrm{b})}. \tag{4.31}$$

The received-power reduction due to ΔL_u is consistent with the RB-based load model in Equation **3.16**. In particular, when the additional path loss is expressed in dB, the received power satisfies

$$P_{u,b}^{(\mathrm{a})}\,(\mathrm{dB}) = P_{u,b}^{(\mathrm{b})}\,(\mathrm{dB}) - \Delta L_u\,(\mathrm{dB}), \tag{4.32}$$

and the equivalent linear-scale relation is

$$P_{u,b}^{(\mathrm{a})} = P_{u,b}^{(\mathrm{b})} \cdot 10^{-\Delta L_u/10} < P_{u,b}^{(\mathrm{b})}. \tag{4.33}$$

To make this SINR reduction explicit, consider the SINR expression in Equation **3.18** together with the following definitions of the interference-plus-noise term. Let

$$\begin{aligned} I_u^{(\mathrm{b})} &\triangleq P_{\mathrm{n}} + \sum_{k \in \mathcal{B}_{\mathrm{act}}^{(\mathrm{b})} \setminus \{b^{(\mathrm{b})}\}} P_{u,k}^{(b)}, \\ I_u^{(\mathrm{a})} &\triangleq P_{\mathrm{n}} + \sum_{k \in \mathcal{B}_{\mathrm{act}}^{(\mathrm{a})} \setminus \{b^{(\mathrm{a})}\}} P_{u,k}^{(a)}, \end{aligned} \tag{4.34}$$

where $I_u^{(\mathrm{b})}$ and $I_u^{(\mathrm{a})}$ denote the interference-plus-noise terms in Equation **3.18** when the serving BS is $b^{(\mathrm{b})}$ and $b^{(\mathrm{a})}$, respectively. For this analytical derivation only, we assume that the aggregate interference-plus-noise term remains nearly unchanged across the switching event, i.e., $I_u^{(a)} \approx I_u^{(b)}$. This assumption is introduced solely to isolate the impact of the additional path-loss term on SINR and does not imply that interference is constant in the general system model. Hence, the SINR values before and after switching are given by

$$\begin{aligned} \gamma_u^{(\mathrm{a})} &= \frac{P_{u,b}^{(\mathrm{a})}}{I_u^{(\mathrm{a})}}, \\ \gamma_u^{(\mathrm{b})} &= \frac{P_{u,b}^{(\mathrm{b})}}{I_u^{(\mathrm{b})}}. \end{aligned} \tag{4.35}$$

Using $P_{u,b}^{(\mathrm{a})} < P_{u,b}^{(\mathrm{b})}$ (from Equation **4.27**) and the assumption $I_u^{(a)} \approx I_u^{(b)}$, it follows that

$$P_{u,b}^{(\mathrm{a})} < P_{u,b}^{(\mathrm{b})} \Rightarrow \gamma_u^{(\mathrm{a})} < \gamma_u^{(\mathrm{b})}. \tag{4.36}$$

This establishes the SINR degradation $\gamma_u^{(\mathrm{a})} < \gamma_u^{(\mathrm{b})}$. The SINR degradation in turn implies a rate degradation. In particular, the achievable rate after switching satisfies

$$R_u^{(\mathrm{a})} = \mathrm{W} \log_2(1 + \gamma_u^{(\mathrm{a})}) < \mathrm{W} \log_2(1 + \gamma_u^{(\mathrm{b})}) = R_u^{(\mathrm{b})}. \tag{4.37}$$

This inequality indicates that cell switching may lead to a degradation in the achievable data rate for certain users. As a result, users whose post-switching rate $R_u^{(\mathrm{a})}$ falls below their rate before cell switching $R_u^{(\mathrm{b})}$ are classified as dissatisfied according to the definition introduced in Equation **4.24**.

Another factor that defines a dissatisfied user is latency. If a user's latency increases after cell switching compared to before the switch, that user is considered dissatisfied. The latency-worsening indicator is defined as

$$\ell_u \triangleq \mathbb{1}\left\{\tau_u^{\mathrm{a}} > \tau_u^{\mathrm{b}}\right\}, \qquad \forall\, u \in \mathcal{U}, \tag{4.38}$$

where τ_u^{a} and τ_u^{b} denote the user latency after and before cell switching, respectively, under the joint ON/OFF and power-level state configuration (Δ, Ω). Accordingly, the number of users whose latency worsens after cell switching is

$$N_\tau \triangleq \sum_{u \in \mathcal{U}} \ell_u. \tag{4.39}$$

To avoid penalizing latency increases, we introduce a latency tolerance parameter $N_{\tau,\max}$, which specifies the maximum number of users allowed to experience latency worsening after cell switching without being counted as dissatisfied due to latency. Latency degradation is therefore considered significant only when the number of users experiencing increased latency exceeds this tolerance threshold, i.e.,

$$N_\tau > N_{\tau,\max}. \tag{4.40}$$

Although switching off underutilized SBSs and operating active SBSs in low-power mode reduces total network power consumption $P(\Delta, \Omega)$, users served by switched-off or power-limited SBSs may be offloaded to the MBS or HIBS, potentially increasing their end-to-end latency. Moreover, when the network reduces power by switching off BSs, many connected users suffer from lower data rates, increasing the number of dissatisfied users, denoted as

$$d_u = \begin{cases} 1, & R_u^{\mathrm{a}} < R_u^{\mathrm{b}} \ \vee \ (\ell_u = 1 \ \wedge \ N_\tau > N_{\tau,\max}), \\ 0, & \text{otherwise}, \end{cases} \tag{4.41}$$

where $d_u = 1$ and $d_u = 0$ represent the user becoming dissatisfied and not dissatisfied, respectively.

In addition to user connectivity and dissatisfaction, the fairness of resource allocation among users should also be considered during cell switching. Even when users remain connected and the average achievable rate is preserved, the after cell switching configuration may still result in highly uneven rate distribution among users. In particular, some users may retain relatively high achievable rates, while others may experience severe degradation due to weaker received signal strength, higher path loss, or increased load on the serving BS. To account for this effect, a fairness-oriented objective is introduced, where the fairness of the achievable rate distribution is quantified using Jain's fairness index.

$$\tilde{R}_u = \begin{cases} R_u, & \text{if user } u \text{ is connected}, \\ 0, & \text{otherwise}. \end{cases} \tag{4.42}$$

The effective rate definition in Equation **4.42** is introduced to ensure that both connected and unserved users are consistently represented in the fairness evaluation. In particular, assigning zero rate to unconnected users enables the fairness metric to jointly reflect both rate distribution and user connectivity. Based on this definition, Jain's fairness index is employed to quantify the uniformity of achievable rates across all users in the network.

$$J(\Delta, \Omega) = \frac{\left(\sum_{u \in U} \tilde{R}_u\right)^2}{|U| \sum_{u \in U} \tilde{R}_u^2}. \tag{4.43}$$

The fairness index provides a normalized measure of the achievable rate distribution among users, taking values in the range $0 < J \leq 1$. A value close to one indicates a highly uniform rate allocation, whereas lower values reflect increasing inequality among users.

Based on the fairness metric, a fairness-oriented optimization problem is formulated to limit the inequality in the achievable rate distribution after cell switching. Since the proposed framework is expressed in a minimization form, the fairness objective is equivalently represented by minimizing the unfairness measure.

$$\begin{aligned} \min_{\Delta,\Omega} \quad & F(\Delta,\Omega) \\ \text{s.t.} \quad & \textbf{(3.21)}, \\ & \textbf{(4.1a) – (4.1c)}, \\ & \textbf{(4.4)}, \\ & \textbf{(4.7)}. \end{aligned} \tag{4.44}$$

The objective function $F(\Delta,\Omega)$ represents the degree of unfairness in the achievable rate distribution. Minimizing this function corresponds to maximizing the fairness index, thereby ensuring a more balanced allocation of network resources among users. The objective function $F(\Delta,\Omega)$ is defined as the complement of the Jain's fairness index, i.e.,

$$F(\Delta,\Omega) = 1 - J(\Delta,\Omega), \tag{4.45}$$

which transforms the fairness maximization problem into an equivalent minimization form. Therefore, minimizing $F(\Delta,\Omega)$ is equivalent to maximizing fairness.

4.3 ϵ-Constraint Method (ϵCM)

In order to jointly address multiple conflicting objectives in the cell switching problem, the ϵCM is adopted. This method transforms the original multi-objective problem into a single-objective formulation by minimizing total power consumption while constraining the remaining objectives using predefined ϵ thresholds. Specifically, HIBS utilization, the number of unconnected users, the number of dissatisfied users, and unfairness in rate distribution are limited through their respective ϵ parameters. Including a HIBS utilization constraint is essential because it constrains how much the network relies on HIBS and prevents excessive use. This allows a better balance among controlled HIBS

usage, energy efficiency, user-centric performance, and fairness.

This method can be formulated by converting the optimization problems in Equation **4.16**, Equation **4.19**, Equation **4.23** and Equation **4.44** into constraints for the problem in Equation **4.9**. Hence, the optimization problem in Equation **4.9** is reformulated as

$$\min_{\Delta,\Omega} \quad P(\Delta,\Omega) \tag{4.46}$$

s.t. **(4.1a) – (4.1c)**,

(4.4),

(4.7).

$$D(\Delta,\Omega) \leq \epsilon_D, \tag{4.46a}$$

$$U(\Delta,\Omega) \leq \epsilon_U, \tag{4.46b}$$

$$H(\Delta,\Omega) \leq \epsilon_H, \tag{4.46c}$$

$$F(\Delta,\Omega) \leq \epsilon_F. \tag{4.46d}$$

In this approach, the conventional energy-focused cell switching problem is preserved as the primary objective, while performance objectives—namely the number of unconnected users, the number of dissatisfied users, the unfairness in rate distribution, and the utilization of HIBS after cell switching—are integrated as bounded constraints. In particular, the HIBS usage objective limits the reliance on HIBS and ensures that it operates as a complementary support layer rather than a primary serving entity. Excessive use of HIBS increases power consumption because as more users connect to it, its load factor increases, leading to higher total power consumption in Equation **4.2**, which challenges the objective in Equation **4.9**. In addition, ϵ-constraints denoted by ϵ_D, ϵ_U, ϵ_H, and ϵ_F are introduced to limit the number of dissatisfied users, limit the number of unconnected users, restrict HIBS utilization, and control unfairness in the rate distribution. By varying the ϵ-values, the formulation provides a controllable trade-off between minimizing power consumption and maintaining user connectivity, service quality, fairness, and bounded HIBS usage.

CHAPTER 5

METHODOLOGY

This chapter presents the methodology adopted to solve the formulated cell switching problem within the ϵ-constraint framework. First, the implementation of the ϵCM is described, including the selection of ϵ parameters to control the trade-off between energy efficiency and user-centric performance metrics. Then, different cell switching algorithms, namely genetic algorithm, greedy approach, and exhaustive search, are introduced to solve the optimization problem. These methods provide a balance between computational complexity and solution optimality, enabling both efficient and accurate evaluation of the proposed framework. In this study, exhaustive search is adopted as the reference method due to the manageable network size, providing an optimal benchmark, while the greedy and genetic algorithms are included for comparison.

5.1 Selection of ϵ Parameters

The ϵ-constraint method transforms the multi-objective problem into a constrained optimization problem of the form

$$\min_{\Delta,\Omega} P(\Delta,\Omega), \tag{5.1}$$

subject to

$$U(\Delta,\Omega) \leq \epsilon_U, \quad D(\Delta,\Omega) \leq \epsilon_D, \quad F(\Delta,\Omega) \leq \epsilon_F, \quad H(\Delta,\Omega) \leq \epsilon_H. \tag{5.2}$$

The selection of the ϵ parameters plays a critical role in determining the trade-off between energy efficiency and user-centric performance metrics. Let

$$\boldsymbol{\epsilon} = (\epsilon_U, \epsilon_D, \epsilon_F, \epsilon_H) \tag{5.3}$$

denote the vector of constraint thresholds.

A set of candidate values is defined for each constraint:

$$\epsilon_k \in \mathcal{E}_k, \quad k \in \{U, D, F, H\}, \tag{5.4}$$

where $\mathcal{E}_k$ denotes the predefined search set for each constraint.

For each configuration $\boldsymbol{\epsilon}$, the optimization problem is solved, yielding the optimal solution pair

$$(\Delta^\star(\boldsymbol{\epsilon}), \Omega^\star(\boldsymbol{\epsilon})). \tag{5.5}$$

The corresponding performance is evaluated as

$$M(\boldsymbol{\epsilon}) = \Big(P(\Delta^\star, \Omega^\star), U(\Delta^\star, \Omega^\star), D(\Delta^\star, \Omega^\star), F(\Delta^\star, \Omega^\star), H(\Delta^\star, \Omega^\star)\Big). \tag{5.6}$$

The selected ϵ values are those that provide a balanced trade-off between power consumption and user-centric performance while ensuring feasibility. Based on this empirical evaluation, all ϵ parameters are set to

$$\epsilon_U = \epsilon_D = \epsilon_F = \epsilon_H = 0.1, \tag{5.7}$$

which represents a moderate constraint level that enables controlled degradation in user-centric metrics while preventing excessive reliance on HIBS resources.

5.2 Cell Switching Algorithms

5.2.1 Genetic Algorithm

The genetic algorithm is employed as a population-based metaheuristic method to explore the solution space efficiently. In this framework, SBS switching and power-level adaptation decisions are jointly represented by

$$\Delta = [\delta_{1,t}, \delta_{2,t}, \ldots, \delta_{\Gamma,t}]^\top \in \{0, 1\}^\Gamma, \tag{5.8}$$

and

$$\Omega = [\rho_{1,t}, \rho_{2,t}, \ldots, \rho_{\Gamma,t}]^\top, \quad \rho_{i,t} \in \{0, 1\}, \tag{5.9}$$

where $\delta_{i,t}$ denotes the ON/OFF state of SBS i, and $\rho_{i,t}$ represents the transmit power-level state of SBS i.

Each chromosome in the population corresponds to a joint decision vector (Δ, Ω).

An initial population

$$\mathcal{P}^{(0)} = \{(\Delta^{(1)}, \Omega^{(1)}), (\Delta^{(2)}, \Omega^{(2)}), \ldots, (\Delta^{(N)}, \Omega^{(N)})\} \tag{5.10}$$

of size N is randomly generated.

For each individual, the fitness function is defined as

$$\mathcal{J}(\Delta, \Omega) = P(\Delta, \Omega), \tag{5.11}$$

where (Δ, Ω) must belong to the feasible solution set $\mathcal{F}$, defined as

$$\mathcal{F} = \{(\Delta, \Omega) \mid U(\Delta, \Omega) \leq \epsilon_U, D(\Delta, \Omega) \leq \epsilon_D, F(\Delta, \Omega) \leq \epsilon_F, H(\Delta, \Omega) \leq \epsilon_H\}. \tag{5.12}$$

Only feasible solutions satisfying the above constraints are considered during the selection process. At each generation g, a new population $\mathcal{P}^{(g+1)}$ is generated through selection, crossover, and mutation operators. Selection favors individuals with lower fitness values, while crossover combines pairs of parent solutions to generate offspring. Mutation introduces random variations in both the activation vector Δ and the power-level vector Ω to enhance exploration of the search space.

The iterative process continues until a stopping criterion is satisfied, such as reaching a maximum number of generations or convergence of the fitness value. The best feasible solution $(\Delta^\star, \Omega^\star)$ obtained across all generations is selected as the final solution.

5.2.2 Greedy-Based Cell Switching

To reduce computational complexity, a greedy-based cell switching algorithm is adopted as a heuristic alternative. In this approach, SBS switching and power-level adaptation decisions are jointly represented by

$$\Delta^{(r)} = [\delta_{1,t}^{(r)}, \delta_{2,t}^{(r)}, \ldots, \delta_{\Gamma}^{(r)}]^{\top}, \tag{5.13}$$

and

$$\Omega^{(r)} = [\rho_{1,t}^{(r)}, \rho_{2,t}^{(r)}, \ldots, \rho_{\Gamma}^{(r)}]^{\top}, \tag{5.14}$$

where $\delta_{i,t}^{(r)} \in \{0, 1\}$ denotes the ON/OFF state of SBS i, and $\rho_{i,t}^{(r)}$ represents its transmit power level.

The greedy algorithm starts from the fully active configuration

$$\Delta^{(0)} = [1, 1, \ldots, 1]^{\top}. \tag{5.15}$$

At each iteration, only active SBSs are considered as candidates for deactivation

$$i : \delta_{i}^{(r)} = 1. \tag{5.16}$$

For each candidate SBS i, a new solution is generated by switching off SBS i

$$\Delta_{-i}^{(r)} = \Delta^{(r)} - \mathbf{e}_i. \tag{5.17}$$

The corresponding power-level vector is updated as

$$\Omega_{-i}^{(r)} = \Omega^{(r)} - \rho_{i,t}^{(r)} \mathbf{e}_i, \tag{5.18}$$

ensuring that inactive SBSs have zero transmit power.

The impact of deactivating SBS i is evaluated as

$$\Delta P_i^{(r)} = P\left(\Delta_{-i}^{(r)}, \Omega_{-i}^{(r)}\right) - P\left(\Delta^{(r)}, \Omega^{(r)}\right). \tag{5.19}$$

The SBS selected for deactivation is determined as

$$i^\star = \arg \min_{i:\delta_{i,t}^{(r)}=1} \Delta P_i^{(r)}, \tag{5.20}$$

subject to the ϵ-constraint conditions

$$U(\Delta_{-i}^{(r)}, \Omega_{-i}^{(r)}) \le \epsilon_U, \quad D(\Delta_{-i}^{(r)}, \Omega_{-i}^{(r)}) \le \epsilon_D, \quad F(\Delta_{-i}^{(r)}, \Omega_{-i}^{(r)}) \le \epsilon_F, \quad H(\Delta_{-i}^{(r)}, \Omega_{-i}^{(r)}) \le \epsilon_H. \tag{5.21}$$

If the selected candidate solution satisfies all constraints, the state is updated as

$$\Delta^{(r+1)} = \Delta^{(r)} - \mathbf{e}_{i^\star}, \quad \Omega^{(r+1)} = \Omega^{(r)} - \rho_{i^\star,t}^{(r)} \mathbf{e}_{i^\star}. \tag{5.22}$$

The iterative process continues until no additional SBS can be switched off without violating the predefined ϵ-constraints. Although this approach significantly reduces computational complexity, it does not guarantee global optimality since decisions are made based on local impact at each iteration.

5.2.3 Exhaustive Search-Based Cell Switching

The exhaustive search approach determines the optimal SBS activation and power-level configuration by evaluating all possible combinations under the given ϵ-constraints. The SBS ON/OFF decisions are represented by

$$\Delta = [\delta_{1,t}, \delta_{2,t}, \ldots, \delta_{\Gamma}]^\top \in \{0,1\}^\Gamma, \tag{5.23}$$

and the corresponding power-level vector is given by

$$\Omega = [\rho_{1,t}, \rho_{2,t}, \ldots, \rho_{\Gamma,t}]^\top, \tag{5.24}$$

where δ_i denotes the activation state of SBS i, and $\rho_{i,t}$ represents its transmit power level.

The joint optimization problem can be formulated as

$$\min_{\Delta,\ \Omega} P(\Delta, \Omega), \tag{5.25}$$

subject to the ϵ-constraint conditions

$$U(\Delta, \Omega) \leq \epsilon_U, \quad D(\Delta, \Omega) \leq \epsilon_D, \quad F(\Delta, \Omega) \leq \epsilon_F, \quad H(\Delta, \Omega) \leq \epsilon_H, \tag{5.26}$$

and the feasibility condition

$$\rho_{i,t} = 0 \quad \text{if } \delta_i = 0. \tag{5.27}$$

The exhaustive search evaluates all possible activation vectors Δ, resulting in a total of 2^Γ candidate configurations. For each configuration, the corresponding power-level vector Ω is determined, and user association is updated based on SINR, resource block availability, and receiver sensitivity constraints. The resulting performance metrics are then computed.

Only feasible solutions satisfying the ϵ-constraints are considered. The optimal solution is obtained as:

$$(\Delta^\star, \Omega^\star) = \arg \min_{(\Delta,\Omega)\in\mathcal{F}} P(\Delta, \Omega), \tag{5.28}$$

where $\mathcal{F}$ denotes the set of feasible solutions satisfying all constraint conditions.

In this study, exhaustive search is adopted as the primary solution method due to its ability to guarantee global optimality. Although the computational complexity grows exponentially with the number of SBSs, i.e., $O(2^\Gamma)$, the network size is sufficiently small to allow exhaustive evaluation. This ensures that the obtained solution represents the true optimal trade-off between energy efficiency and user-centric performance.

CHAPTER 6

PERFORMANCE EVALUATION

This section evaluates the performance of the proposed cell switching framework using two complementary analyses. First, MATLAB-based system-level simulations are used to examine the proposed ϵCM framework in terms of achievable data rate and power consumption under different network conditions. Then, a Python-Sionna-OAI-based implementation is considered to validate the practical applicability of the proposed approach. While the MATLAB results provide a detailed performance analysis, the OAI-based results demonstrate that the proposed framework can be implemented in a practical RAN setting. The following results present the impact of the proposed framework on achievable data rate and network power consumption, as well as its behavior in an OAI-based environment.

6.1 Performance Metrics

The evaluation of the proposed cell switching framework is based on three key metrics: achievable data rate, total network power consumption, and HIBS utilization. These metrics capture both user-centric performance and system-level efficiency in heterogeneous TN–NTN systems.

6.1.1 Achievable Data Rate

The achievable data rate is used as the primary user-centric performance metric. It reflects the QoS experienced by users under different propagation conditions and cell switching strategies. The achievable rate depends on SINR, resource allocation, and propagation effects such as BEL. This metric is evaluated for different user categories, including high-loss indoor, low-loss indoor, and outdoor users.

6.1.2 Total Network Power Consumption

Total network power consumption is used to quantify the energy efficiency of the network. It includes the power consumed by all active BSs, including SBSs, MBS, and HIBS. This metric enables the evaluation of how effectively the proposed framework

reduces energy consumption through cell switching and transmit power scaling under varying traffic conditions.

6.1.3 HIBS Utilization

HIBS utilization represents the extent to which the non-terrestrial layer is used to support the network. It is quantified in terms of the number of users connected to HIBS. This metric is particularly important in the proposed framework, as excessive reliance on HIBS is controlled through the H constraint. Therefore, it provides insight into how the framework balances terrestrial and non-terrestrial resources.

6.2 Benchmark Models

The models and configurations used to evaluate the proposed ϵCM-based cell switching framework are introduced. These include baseline models, different SBS operating strategies, and solution algorithms, enabling a comprehensive comparison in terms of energy efficiency, user-centric performance, and HIBS utilization.

6.2.1 Baseline Model: EFM

The EFM is used as the primary baseline. In this model, cell switching decisions are made solely to minimize total network power consumption without considering user-centric performance metrics or HIBS utilization constraints. This benchmark enables the evaluation of how the proposed framework improves performance while maintaining energy efficiency.

6.2.2 SBS Operating Modes

Two switching strategies are considered to analyze their impact: ON/OFF switching and FULL/LOW transmit power scaling. In the ON/OFF strategy, SBSs are either fully active or switched off, whereas the FULL/LOW strategy allows them to operate at reduced power for more gradual switching. This comparison highlights the trade-offs between aggressive and controlled switching.

6.2.3 Cell Switching Algorithms

Different algorithms are considered to solve the cell switching problem within the proposed framework, including exhaustive search, greedy approach, and genetic algorithm. The exhaustive search provides the optimal solution but suffers from high computational complexity, while the greedy and genetic algorithms offer near-optimal performance with significantly reduced complexity. These approaches are compared to demonstrate the effectiveness and practicality of the proposed framework.

6.3 Simulation Results

Network performance under different propagation conditions is evaluated by analyzing the achievable data rate for BEL values ranging from 0 to 30 dB [2]. Since atmospheric attenuation exhibits negligible variation over the considered scenario, it is treated as a constant, allowing the analysis to primarily focus on the impact of BEL. To capture propagation-aware user behavior, three user categories are defined: high-loss indoor, low-loss indoor, and outdoor users. High-loss indoor users experience significant additional attenuation beyond BEL, whereas low-loss indoor users are subject to reduced entry loss as defined in Equation **3.5**. In contrast, outdoor users are assumed to be unaffected by BEL. Each user is assigned one RB, resulting in a fixed traffic demand per user across all simulation intervals and collectively forming the overall network load. These propagation characteristics and traffic assumptions directly influence the achievable data rates, which in turn affect user association and cell switching decisions throughout the network.

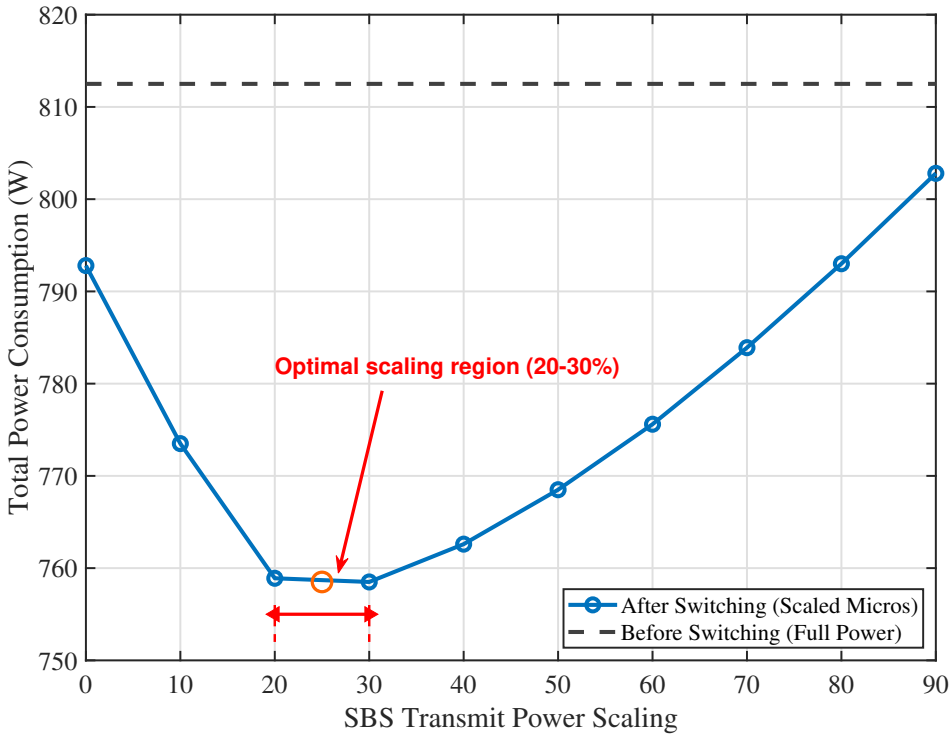


Figure 6.1 SBS transmit power scaling.

Fig. 6.1 illustrates the impact of SBS transmit power scaling on the total network power consumption. The baseline case represents the network before cell switching where all BSs operate at full transmit power and the total power consumption remains around 810 W. The proposed cell switching with scaled SBSs demonstrates a non-linear behavior. As the transmit power scaling factor decreases from full power to around 20–30%, the total power consumption is reduced, reaching its minimum value. This reduction is achieved by lowering transmission power while still allowing SBSs to serve a portion of the users, which reduces the load on MBS and HIBS. Importantly, operating at 20–30% scaling is more energy-efficient than the 0% scaling case, where SBSs become effectively inactive. In the 0% scaling scenario, users are forced to connect to higher-power layers such as MBS or HIBS, which increases the overall network load and consequently the total power consumption. However, beyond the optimal scaling region further reduction in transmit power degrades signal quality and user association, leading to increased power consumption. These results highlight that, within the proposed cell switching framework, an optimal transmit power scaling level exists that balances energy efficiency and network performance. Moreover, controlled

low-power operation of SBSs is more effective than complete switching off.

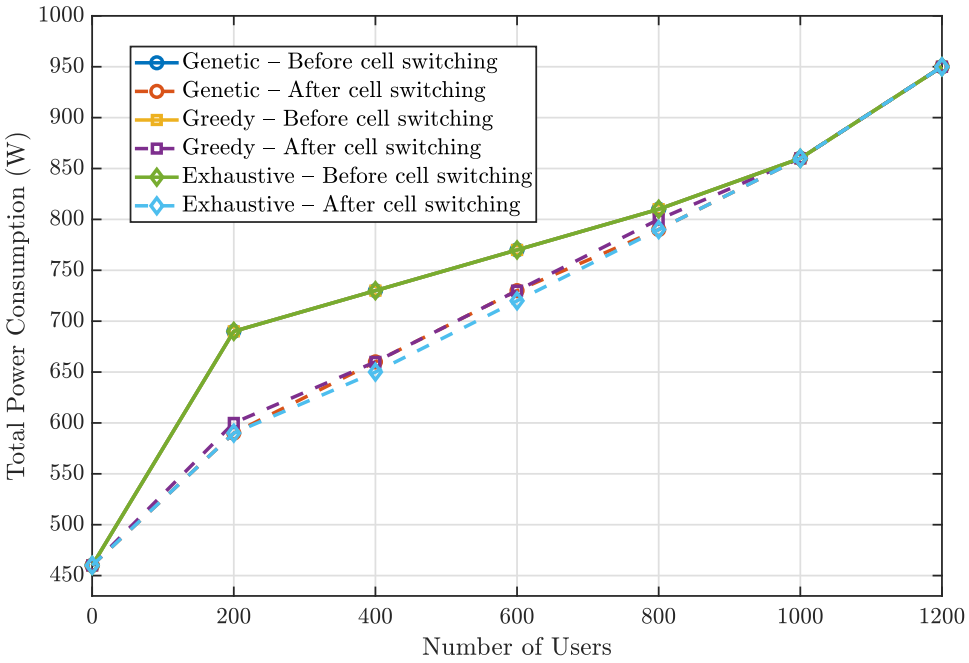


Figure 6.2 Total network power consumption of the ϵCM method with three different methodologies (i.e., genetic algorithm, greedy approach, and exhaustive search).

Fig. 6.2 presents a comparative evaluation of three cell switching strategies within the ϵCM framework, namely exhaustive search, greedy approach, and genetic algorithm. The exhaustive search method determines the optimal SBS activation pattern by evaluating all possible ON/OFF combinations under the given ϵ-constraints. However, its computational complexity increases exponentially with the number of SBSs ($O(2^{\Gamma})$), which makes it impractical for large-scale deployments. To address this limitation, two heuristic approaches are considered. In particular, the greedy algorithm iteratively deactivates SBSs with the smallest impact on the objective function, resulting in near-optimal performance with much lower computational complexity. Meanwhile, the genetic algorithm uses a population-based metaheuristic approach in which each candidate corresponds to an SBS activation pattern, enabling the identification of high-quality solutions without checking each possible SBS configuration.

As shown in Fig. 6.2, all three methods show a similar trend in total network power consumption as the number of users increases. The greedy and genetic algorithms

perform close to the exhaustive search, indicating that near-optimal solutions can be achieved with much lower computational complexity. In this study, exhaustive search is used as the reference method due to the small network size, providing an optimal benchmark, while the greedy and genetic algorithms are included for comparison.

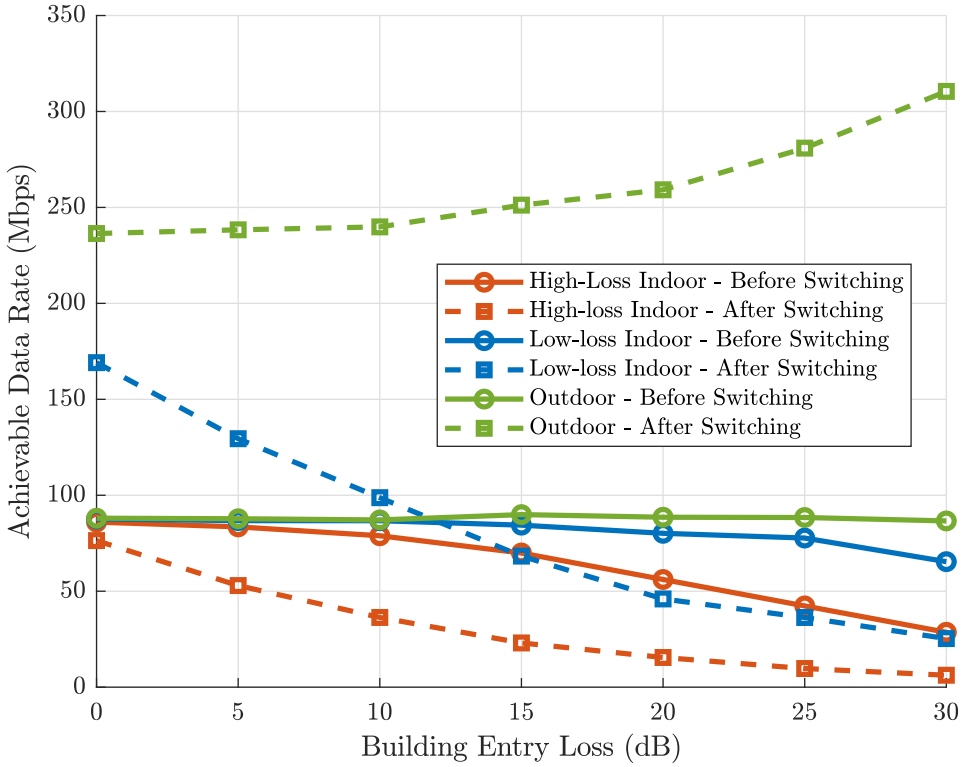


Figure 6.3 Achievable data rate of EFM under varying BEL conditions.

Fig. 6.3 demonstrates the achievable data rate performance under varying BEL conditions before and after applying the EFM-based cell switching. As BEL increases, achievable data rates for high-loss indoor users decline significantly due to their high vulnerability to propagation loss effects. In contrast, cell switching slightly improves the performance of low-loss indoor users as switching certain BSs reduces the interference term in the SINR expression, leading to higher achievable data rates. However, this improvement is limited to moderate BEL values. Beyond approximately 10-15 dB, the impact of BEL dominates the interference reduction, resulting in a gradual decrease in achievable rates. On the other hand, outdoor users consistently experience improved performance after cell switching, as they are not affected by BEL and the reduction in interference leads to higher SINR values. Furthermore,

increasing BEL causes more indoor users to become weakly connected or unserved, which makes additional RBs available at the MBS and HIBS. This allows outdoor users to utilize more RBs and achieve higher data rates particularly beyond 20 dB BEL. In general, the results highlight that the impact of cell switching is user-dependent and is jointly influenced by propagation conditions, interference dynamics, and resource redistribution. This indicates the importance of propagation-aware cell switching strategies in heterogeneous environments.

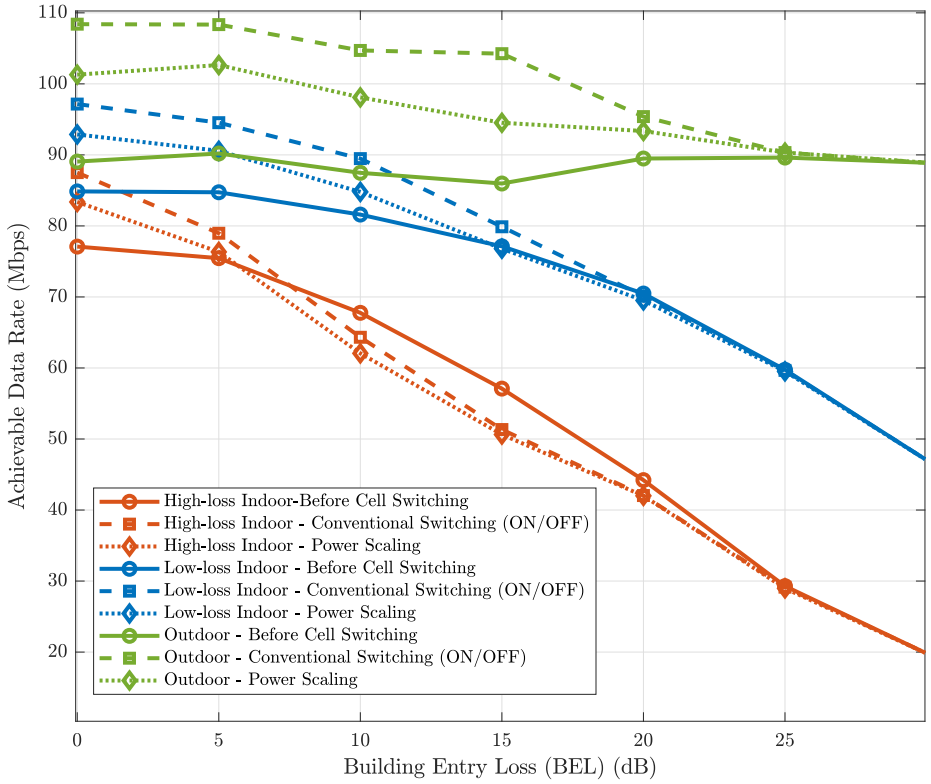


Figure 6.4 Achievable data rate of ϵCM under varying BEL conditions.

Fig. 6.4 illustrates the achievable data rate performance of the ϵCM framework under different BEL conditions. For high-loss indoor users, cell switching slightly improves achievable data rates at low BEL levels, particularly up to around 10 dB. In this region, reducing the number of active BSs reduces interference, which improves SINR and enhances user performance. However, as BEL increases, the combined effect of BEL and BS deactivation causes a gradual decline in their achievable data rates. Meanwhile, low-loss indoor users experience a slight increase in achievable data rates and remain relatively stable up to around 25 dB BEL. Beyond this level, their rates remain nearly

unchanged, as they are less sensitive to BEL. Outdoor users consistently maintain high data rates, as they are not affected by BEL and benefit directly from interference reduction. In general, the results show that the performance of ϵCM depends on the balance between BEL, interference reduction, and BS switching off, leading to different performance trends for users under varying BEL levels.

Fig. 6.4 also demonstrates the achievable data rate performance under the FULL/LOW (%20 transmit power scaling) strategy within the ϵCM framework. Unlike the ON/OFF approach, this strategy operates SBSs at lower power, resulting in a more gradual cell switching behavior. For high-loss indoor users, data rates decrease as BEL increases, but the drop is less severe than in the ON/OFF case because low-power SBSs continue to provide partial coverage and maintain performance. Similarly, low-loss indoor users experience a smoother decline in performance, as low-power SBSs help maintain connectivity and reduce the impact of aggressive cell switching. This more moderate performance degradation comes from the fact that SBSs remain partially active and continue to provide useful signal power, even though the interference reduction is smaller than in the ON/OFF case. As a result, the performance gains are generally smaller in the FULL/LOW case. Since SBSs operating at 20% transmit power still contribute to the interference level in the network, the SINR improvement remains limited, leading to more limited performance improvements in achievable data rates across user types. Overall, these results show that operating SBSs at reduced power provides a more stable and gradual performance behavior, although it limits the achievable data rate gains compared to the ON/OFF strategy.

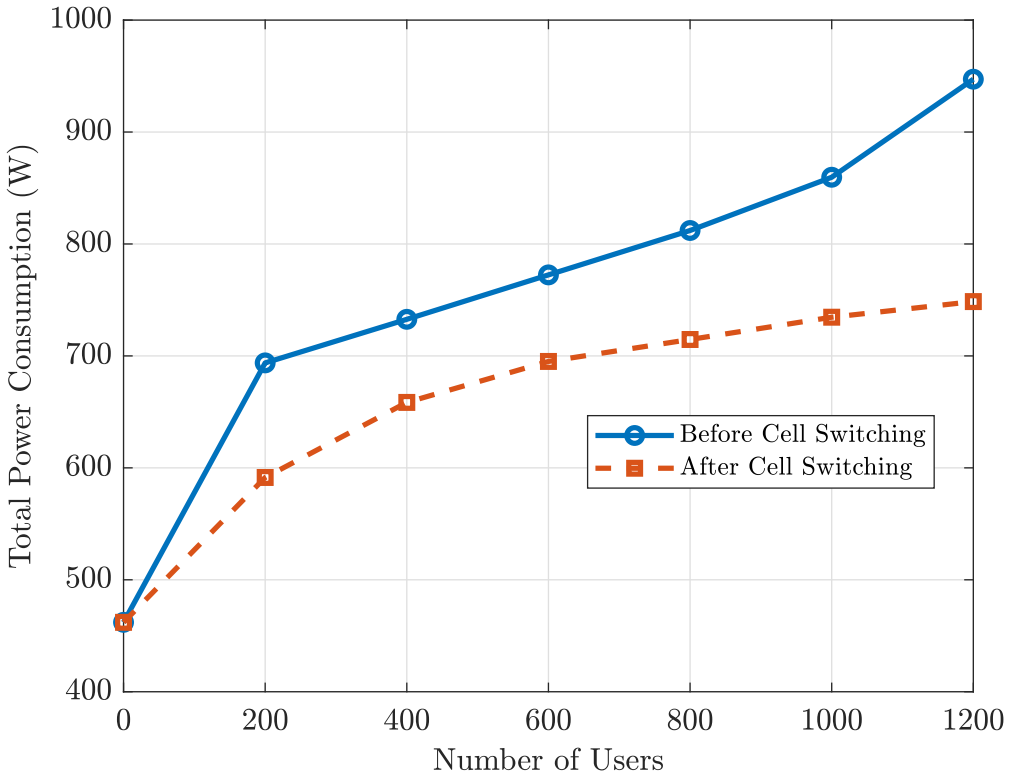


Figure 6.5 Total power consumption of EFM under different user densities.

Fig. 6.5 presents the total power consumption under different user densities for the EFM, comparing network operation before and after cell switching. As the number of users increases, the total power consumption rises in both cases due to the higher traffic demand and the increased load on active BSs. However, after cell switching is applied, power consumption remains lower across all user densities. This reduction is achieved by switching off underutilized SBSs and offloading traffic to a smaller set of active BSs, particularly the MBS and HIBS. Beyond a certain user density, the network reaches a near-optimal set of active BSs, which limits further switching. As a result, additional users are mostly served by the already active BSs, leading to a more gradual increase in power consumption after switching. Nevertheless, even at high user densities, EFM still achieves noticeable power savings compared to the case before cell switching. Overall, these results show that EFM demonstrates adaptive behavior under varying traffic conditions, although the flexibility of switching becomes more limited as user demand increases.

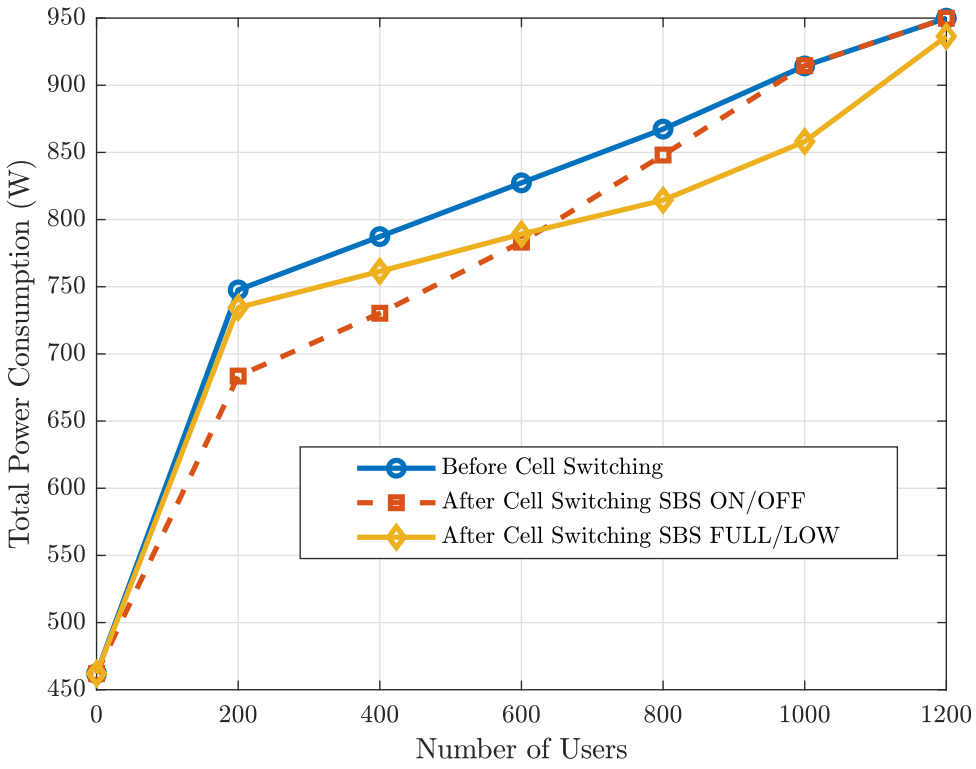


Figure 6.6 Total power consumption of ϵCM under different user densities.

Fig. 6.6 illustrates the total power consumption under different user densities within the ϵCM framework and presents the network behavior before and after cell switching. As expected, the power consumption increases with the number of users in both scenarios due to the higher traffic demand and increased load on the network. However, in contrast to the EFM, the reduction achieved after cell switching is more constrained. This is because the ϵCM framework incorporates multiple constraints, including H, U, D, and F, which limit excessive BS switching off. In particular, while switching off SBSs reduces power consumption, the ϵ-constraints prevent extensive switching off that would compromise user connectivity and quality-of-service requirements. The H constraint limits excessive reliance on HIBS, while the U constraint keeps the number of unconnected users within a defined threshold. The D constraint limits the number of users experiencing rate degradation after cell switching. In addition, the F constraint ensures that this degradation is not concentrated among a small subset of users, thereby maintaining a balanced performance distribution. As user density increases, these constraints become increasingly restrictive, since maintaining connectivity, fairness, and user performance requires more BSs to remain active. As a result, the achievable

power reduction decreases at higher user densities. Overall, the results show that the ϵCM approach provides controlled and user-aware energy savings while maintaining connectivity, fairness, and balanced use of HIBS resources.

In addition, Fig. 6.6 compares the total power consumption of the ON/OFF and FULL/LOW (%20 transmit power scaling) cell switching strategies under varying user densities within the ϵCM framework. In both approaches, power consumption increases with the number of users due to the rising traffic demand. However, up to around 600 users, the FULL/LOW approach results in higher power consumption compared to the ON/OFF strategy, as SBSs remain active at reduced transmit power instead of being completely switched off, thereby increasing baseline power consumption. Conversely, beyond approximately 600 users, the FULL/LOW strategy tends to achieves lower power consumption than the ON/OFF approach. As user density increases, the ϵ-constraints on connectivity, rate degradation, fairness, and HIBS utilization become more restrictive, so the ON/OFF strategy needs to keep more SBSs active to satisfy these requirements. Under these conditions, the FULL/LOW approach becomes more efficient, as it can maintain user performance with partially active SBSs without fully reactivating them. As a result, this reduces the need to fully reactivate SBSs, leading to lower overall power consumption.

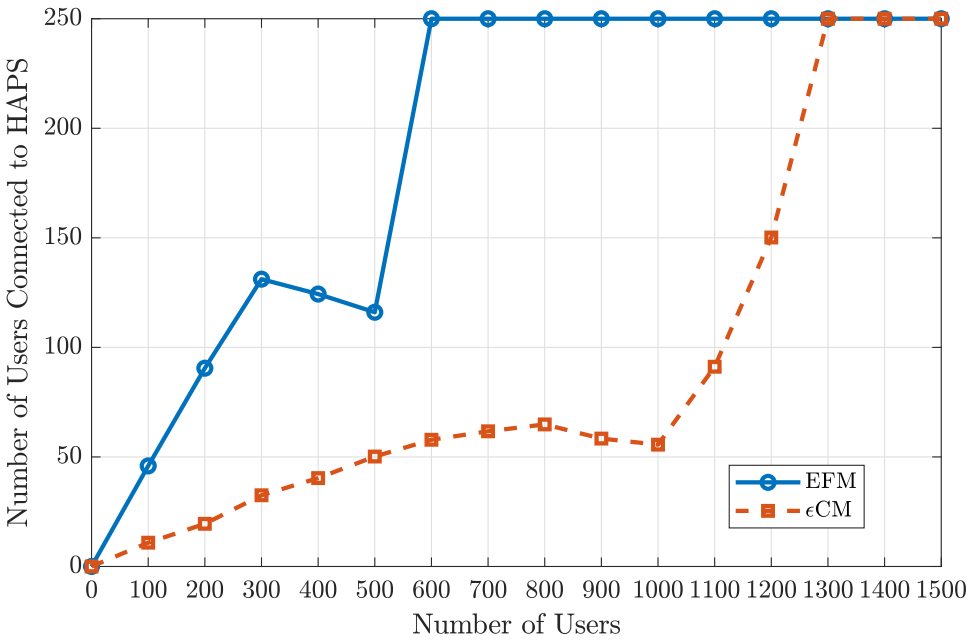


Figure 6.7 Number of users connected to HIBS under the EFM and ϵCM frameworks.

Fig. 6.7 presents the number of users connected to HIBS within the EFM and ϵCM methods. The EFM aggressively offloads users to HIBS, leading to higher HIBS utilization at low and moderate user densities, as it prioritizes energy minimization without accounting for other constraints. The temporary decrease in HIBS utilization between 300 and 500 users can be attributed to a shift in the cell switching pattern. At these intermediate loads, keeping some SBSs active becomes more energy-efficient than further increasing HIBS offloading, resulting in a short-term reduction in HIBS usage. When the number of users reaches 600, HIBS utilization saturates, indicating that the HIBS has reached its maximum user capacity defined by the system model. In contrast, the proposed ϵCM framework maintains controlled HIBS utilization by applying user-centric constraints. However, beyond approximately 1000 users, the system approaches its feasibility limits, as maintaining user performance and connectivity becomes increasingly challenging. As a result, the ϵCM framework increases HIBS utilization to satisfy these constraints, resulting in a sharp increase in the number of HIBS-associated users. At very high user densities of around 1300 users, both approaches converge to similar HIBS utilization levels, indicating that HIBS becomes an essential component under heavy load conditions, regardless of the optimization strategy.

6.4 Python–Sionna–OAI-Based Performance Evaluation

This section presents the performance evaluation of the proposed ϵCM framework within a system-level setting. To capture both the optimization method and its impact on network behavior, a Python–Sionna–OAI architecture is used. In this structure, Python acts as the main control layer, coordinating the interaction between link-level modeling and network-level decisions. Sionna provides physical-layer information, including channel conditions and SINR, which supports user-centric decision making. Using these inputs, Python evaluates the ϵ-constraints and determines the appropriate cell switching decisions. Meanwhile, OAI represents how these decisions are implemented at the network level through user reassociation and resource allocation. In this way, the framework allows us to observe both power consumption and the resulting changes in user distribution and overall network behavior.

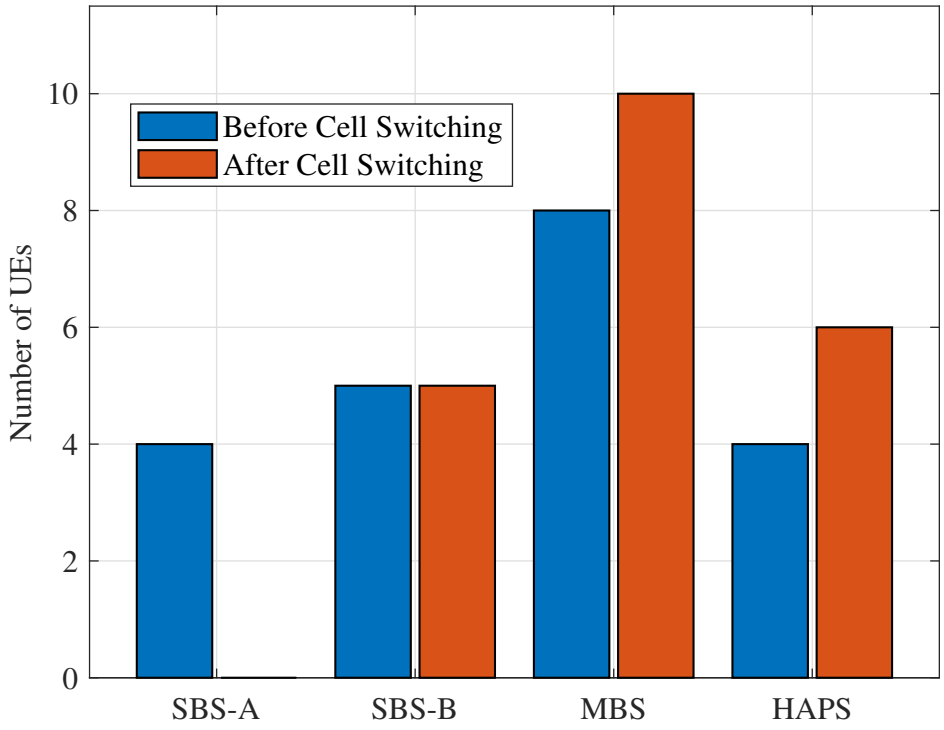


Figure 6.8 User distribution across BSs before and after cell switching in the simplified Python–Sionna–OAI framework.

Fig. 6.8 presents a simplified scenario with four BSs and a small number of users to illustrate how the proposed cell switching framework operates in the Sionna–OAI environment. This simplified framework is used to highlight the decision-making process while keeping the computational complexity low. Before cell switching, users are distributed across SBS-A, SBS-B, MBS and the HIBS according to the association policy. After applying cell switching, the framework identifies SBS-A as the least-loaded SBS and switches it off. Consequently, the users previously served by this SBS are redistributed to the MBS and the HIBS. Although the HIBS load increases after switching, it remains within the limits imposed by the H constraint, which allows HIBS usage but limits excessive reliance on it. In general, this example shows how the Sionna–OAI integration captures both SINR feasibility and network-level behavior, enabling a joint evaluation of link-level constraints and system-level load redistribution. Finally, further implementation-level evidence from the OAI environment is provided in Fig A.1.

In general, the performance evaluation demonstrates that the proposed ϵCM framework effectively balances energy efficiency, user-centric performance, and controlled HIBS utilization in heterogeneous TN–NTN networks. The MATLAB-based results reveal that the ϵCM framework regulates HIBS utilization and balances the trade-off by applying constraints on unconnected users, dissatisfied users, and fairness, preventing both performance degradation and excessive use of NTN resources. Furthermore, the Python–Sionna–OAI integration validates that the proposed framework is both theoretically sound and practically implementable, and captures link-level effects and network-level dynamics such as user reassociation and resource allocation.

CHAPTER 7

CONCLUSION

This thesis addressed the limitations of EFM by proposing a propagation- and rate-aware bounded-NTN cell switching framework for HIBS-assisted wireless networks. Rather than solely minimizing total network power, the problem was reformulated as a constrained multi-objective optimization model that balanced user-centric performance metrics with power consumption, while also explicitly limiting excessive HIBS utilization. More specifically, the framework included constraints on U, D, F, and H, so as to control the amount of non-terrestrial resources used. In addition, the model incorporated realistic propagation effects, including BEL and atmospheric attenuation, to capture their impact on user experience. The optimization problem was solved using the ϵCM, which allowed for a flexible and controlled trade-off between performance metrics and energy efficiency while maintaining the complementary role of HIBS in the network. In this context, the proposed framework contributed to more sustainable network operation by improving energy efficiency while preserving user-centric performance.

The results demonstrated that while EFM reduced total network power consumption, it often led to significant degradation in achievable data rates, especially for indoor users under high BEL conditions. For example, under EFM, high-loss indoor users experienced up to 73% degradation, while low-loss indoor users experienced around 43%. The proposed framework effectively mitigated this degradation, reducing it to about 4% for high-loss indoor users and nearly eliminating it for low-loss indoor users, while still providing additional energy savings. However, energy efficiency gains gradually saturated as user density increased, indicating a fundamental limitation caused by capacity and QoS constraints. Furthermore, the analysis indicated that excessive reliance on HIBS could degrade both performance and overall efficiency, whereas the proposed bounded approach ensured more balanced NTN resource usage and reduced HIBS utilization by up to 80% at moderate user densities. Joint optimization of energy efficiency and user-centric performance metrics therefore provided a comprehensive

and practical framework for future TN–NTN architectures in 6G systems.

In addition to the optimization framework, the hybrid Python–Sionna–OAI architecture provided a practical implementation dimension to this study by connecting optimization, link-level wireless modeling, and network-level implementation. While Python enabled the decision-making and optimization process, Sionna provided realistic channel and SINR modeling, and OAI reflected the resulting network behavior through user reassociation and resource allocation. This hybrid structure extended the study beyond conventional simulation-only analysis and highlighted the practical applicability of the proposed framework in more realistic integrated TN–NTN environments.

Beyond quantitative improvements, this study emphasized the need to move beyond purely energy-driven optimization in future integrated TN–NTN systems. The findings indicated that focusing solely on energy minimization could result in a higher number of unconnected users, performance degradation, unfair resource distribution, and excessive reliance on non-terrestrial resources. By incorporating user-centric constraints and realistic propagation conditions, the proposed framework enabled a more balanced decision-making approach that better reflected the practical requirements of next-generation wireless systems. More broadly, the proposed framework supported sustainable HIBS-assisted network design for future 6G architectures. As NTN integration became increasingly important for enabling ubiquitous connectivity, resilient communications, and extended coverage, intelligent management of terrestrial and non-terrestrial resources became essential. In this context, jointly optimizing energy efficiency and user-centric performance offered a practical and scalable approach for future TN–NTN architectures in 6G systems.

CHAPTER 8

FUTURE WORK

An important future research direction is to investigate scalable distributed or hierarchical decision-making architectures for the proposed cell switching framework. This thesis considered cell switching decisions from a centralized optimization perspective, assuming access to global network information. However, in large-scale integrated TN–NTN deployments, centralized control may lead to high computational and signaling overhead, increased decision latency, and scalability challenges. Therefore, a distributed or hierarchical decision-making approach may provide a more scalable and practical implementation, where local BS clusters or NTN-assisted controllers handle part of the optimization process while aiming to preserve energy efficiency and user-centric performance.

REFERENCES

[1] Giordani M. and Zorzi M., “Non-terrestrial networks in the 6G era: Challenges and opportunities,” *IEEE network*, vol. 35, no. 2, pp. 244–251, 2020.

[2] ITU-R, “Compilation of measurement data relating to building entry loss,” ITU Radiocommunication Sector, Tech. Rep. Report ITU-R P.2346-3, May 2019.

[3] International Telecommunication Union (ITU), “The ITU-R framework for IMT-2030,” https://www.itu.int/en/ITU-R/study-groups/rsg5/rwp5d/imt-2030/Pages/default.aspx, July 2023, retrieved April 25, 2026, from https://www.itu.int/en/ITU-R/study-groups/rsg5/rwp5d/imt-2030/Pages/default.aspx.

[4] Alam M. S., Siddiqui S. T., Qidwai K. A., Aftab A., Kamal M. S., and Shahi F. I., “Evolution of wireless communication networks from 5G to 6G: future perspective,” *Radioelectronics and communications systems*, vol. 66, no. 5, pp. 213–222, 2023.

[5] Abbasi O., Yadav A., Yanikomeroglu H., Đào N.-D., Senarath G., and Zhu P., “HAPS for 6G networks: Potential use cases, open challenges, and possible solutions,” *IEEE Wireless Communications*, vol. 31, no. 3, pp. 324–331, 2024.

[6] Kurt G. K., Khoshkholgh M. G., Alfattani S., Ibrahim A., Darwish T. S., Alam M. S., Yanikomeroglu H., and Yongacoglu A., “A vision and framework for the high altitude platform station (HAPS) networks of the future,” *IEEE Communications Surveys & Tutorials*, vol. 23, no. 2, pp. 729–779, 2021.

[7] Harounabadi M. and Heyn T., “Toward integration of 6G-NTN to terrestrial mobile networks: Research and standardization aspects,” *IEEE Wireless Communications*, vol. 30, no. 6, pp. 20–26, 2023.

[8] Ozturk M., Salamatmoghadasi M., and Yanikomeroglu H., “Integrating terrestrial and non-terrestrial networks for sustainable 6G operations: A latency-aware multi-tier cell-switching approach,” *IEEE Network*, 2025.

[9] Alam M. S., Kurt G. K., Yanikomeroglu H., Zhu P., and Đào N. D., "High altitude platform station based super macro base station constellations," *IEEE Communications Magazine*, vol. 59, no. 1, pp. 103–109, 2021.

[10] International Telecommunication Union (ITU), "High-altitude platform systems (HAPS)," https://www.itu.int/en/mediacentre/backgrounders/Pages/High-altitude-platform-systems.aspx, n.d.,Retrieved April 25, 2026.

[11] Kumar R., Gupta S. K., Wang H.-C., Kumari C. S., and Korlam S. S. V. P., "From efficiency to sustainability: Exploring the potential of 6G for a greener future," *Sustainability*, vol. 15, no. 23, p. 16387, 2023.

[12] Feng M., Mao S., and Jiang T., "Base station ON-OFF switching in 5G wireless networks: Approaches and challenges," *IEEE Wireless Communications*, vol. 24, no. 4, pp. 46–54, 2017.

[13] International Telecommunication Union (ITU), "ITU statistics," https://www.itu.int/en/ITU-D/Statistics/pages/stat/default.aspx, 2025, retrieved April 25, 2026, from https://www.itu.int/en/ITU-D/Statistics/pages/stat/default.aspx.

[14] Kamel M., Hamouda W., and Youssef A., "Ultra-dense networks: A survey," *IEEE Communications surveys & tutorials*, vol. 18, no. 4, pp. 2522–2545, 2016.

[15] Ozturk M., Abubakar A. I., Nadas J. P. B., Rais R. N. B., Hussain S., and Imran M. A., "Energy optimization in ultra-dense radio access networks via traffic-aware cell switching," *IEEE Transactions on Green Communications and Networking*, vol. 5, no. 2, pp. 832–845, 2021.

[16] Yu N., Miao Y., Mu L., Du H., Huang H., and Jia X., "Minimizing energy cost by dynamic switching on/off base stations in cellular networks," *IEEE Transactions on Wireless Communications*, vol. 15, no. 11, pp. 7457–7469, 2016.

[17] Wu J., Zhang Y., Zukerman M., and Yung E. K.-N., "Energy-efficient base-stations sleep-mode techniques in green cellular networks: A survey," *IEEE communications surveys & tutorials*, vol. 17, no. 2, pp. 803–826, 2015.

[18] Arvaje F. R. and Ghahfarokhi B. S., "A spectrum efficient base station switching-off mechanism for green cellular networks," in *2017 7th International Conference on Computer and Knowledge Engineering (ICCKE)*, 2017, pp. 433–438.

[19] Oh E., Son K., and Krishnamachari B., "Dynamic base station switching-on/off strategies for green cellular networks," *IEEE Transactions on Wireless Communications*, vol. 12, no. 5, pp. 2126–2136, 2013.

[20] Marsan M. A., Chiaraviglio L., Ciullo D., and Meo M., "On the effectiveness of single and multiple base station sleep modes in cellular networks," *Computer Networks*, vol. 57, no. 17, pp. 3276–3290, 2013.

[21] Kumar A. and Rosenberg C., "Energy and throughput trade-offs in cellular networks using base station switching," *IEEE Transactions on Mobile Computing*, vol. 15, no. 2, pp. 364–376, 2015.

[22] Abubakar A. I., Mollel M. S., Ozturk M., and Ramzan N., "A secured energy saving with federated assisted modified actor-critic framework for 6G networks," *IEEE Transactions on Vehicular Technology*, vol. 74, no. 6, pp. 9671–9688, 2025.

[23] Khorasani S. K., Ghahfarokhi B. S., and Movahhedinia N., "UAVs for qos or energy drain? A study on energy reduction capability of UAV-assisted cell switching scenarios in 6G," *IEEE Access*, 2026.

[24] Renga D. and Meo M., "Can high altitude platform stations make 6G sustainable?" *IEEE Communications Magazine*, vol. 60, no. 9, pp. 75–80, 2022.

[25] Meo M., Renga D., and Scarpa F., "Integrating aerial base stations for sustainable urban mobile networks," in *GLOBECOM 2022 - 2022 IEEE Global Communications Conference*, 2022, pp. 1727–1733.

[26] Kement C. E., Kara F., Jaafar W., Yanikomeroglu H., Senarath G., Dao N. D., and Zhu P., "Sustaining dynamic traffic in dense urban areas with high altitude platform stations (HAPS)," *IEEE Communications Magazine*, vol. 61, no. 7, pp. 150–156, 2023.

[27] Salamatmoghadasi M., Mehrabian A., and Yanikomeroglus H., "Energy sustainability in dense radio access networks via high altitude platform stations," *IEEE Networking Letters*, vol. 6, no. 1, pp. 21–25, 2024.

[28] Koç G. B., Çiloğlu B., Öztürk M., and Yanikomeroglu H., "HAPS-enabled sustainability provision in cellular networks through cell-switching," in *2023 IEEE International Black Sea Conference on Communications and Networking (BlackSeaCom)*, 2023, pp. 294–299.

[29] Koç G. B., Çiloğlu B., Ozturk M., and Yanikomeroglu H., "A lightweight machine learning approach for delay-aware cell-switching in 6G HAPS networks," in *2024 IEEE International Conference on Communications Workshops (ICC Workshops)*, 2024, pp. 1517–1522.

[30] Song T., Lopez D., Meo M., Piovesan N., and Renga D., "High altitude platform stations: the new network energy efficiency enabler in the 6G era," in *2024 IEEE Wireless Communications and Networking Conference (WCNC)*, 2024, pp. 1–6.

[31] Çiloğlu B., Koç G. B., Ozturk M., and Yanikomeroglu H., "Cell switching in HAPS-aided networking: How the obscurity of traffic loads affects the decision," *IEEE Transactions on Vehicular Technology*, vol. 73, no. 11, pp. 17 782–17 787, 2024.

[32] Salamatmoghadasi M., Ozturk M., and Yanikomeroglu H., "Enhancing sustainability in HAPS-assisted 6G networks: Load estimation aware cell switching," in *2025 IEEE 36th International Symposium on Personal, Indoor and Mobile Radio Communications (PIMRC)*. IEEE, 2025, pp. 1–6.

[33] Salamatmoghadasi M., Ozturk M., and Yanikomeroglu H., "Two-phase cell switching in 6G vhetnets: Sleeping-cell load estimation and renewable-aware switching toward NES," *IEEE Transactions on Cognitive Communications and Networking*, vol. 12, pp. 7034–7047, 2026.

[34] Salamatmoghadasi M., Mehrabian A., Yanikomeroglu H., and Kaddoum G., "Sustainable vertical heterogeneous networks: A cell switching approach with

high altitude platform station," *IEEE Transactions on Green Communications and Networking*, 2026.

[35] Öztürk M., "Cell switching in 6G networks for improved sustainability and handover management," *Journal of Turkish Operations Management*, vol. 9, no. 1, p. 201–214, 2025. [Online]. Available: https://izlik.org/JA54PE93ZW

[36] 3GPP, "Study on New Radio (NR) to support non-terrestrial networks," 3rd Generation Partnership Project (3GPP), Tech. Rep. TR 38.811, Sep. 2020.

[37] International Telecommunication Union (ITU-R), "Attenuation by atmospheric gases," ITU Radiocommunication Sector, Tech. Rep. Recommendation ITU-R P.676-9, Feb. 2012.

[38] Auer G., Giannini V., Desset C., Godor I., Skillermark P., Olsson M., Imran M. A., Sabella D., Gonzalez M. J., Blume O., and Fehske A., "How much energy is needed to run a wireless network?" *IEEE Wireless Communications*, vol. 18, no. 5, pp. 40–49, 2011.

APPENDICES

Appendix A: Additional OAI Validation Results.

Appendix A – Additional OAI Validation Results

```
[0m[HW]     Client connects from ::ffff:127.0.0.1:52410
[0m[32m[HW]     RFsim: Number of antennas changed from 0 to 1
[0m[HW]     Client connects from ::ffff:127.0.0.1:53946
[0m[32m[HW]     RFsim: Number of antennas changed from 0 to 1
[0m[NR_MAC] Frame.Slot 0.0
UE RNTI a298 CU-UE-ID 1 in-sync PH 48 dB PCMAX 20 dBm, average RSRP -44 (16 meas)
UE a298: dlsch_rounds 6/0/0/0, dlsch_errors 0, pucch0_DTX 0, BLER 0.06561 MCS (0) 0 CCE fail 4
UE a298: ulsch_rounds 46/0/0/0, ulsch_errors 0, ulsch_DTX 0, BLER 0.00120 MCS (0) 0 (Qm 2 deltaMCS 0 dB) NPRB 5  SNR 50.5 dB CCE fail 0
UE a298: MAC:    TX            85 RX            872 bytes
UE a298: LCID 1: TX             3 RX             41 bytes
UE RNTI 8e17 CU-UE-ID 2 in-sync PH 48 dB PCMAX 20 dBm, average RSRP -44 (16 meas)
UE 8e17: dlsch_rounds 5/0/0/0, dlsch_errors 0, pucch0_DTX 0, BLER 0.07290 MCS (0) 0 CCE fail 3
UE 8e17: ulsch_rounds 41/0/0/0, ulsch_errors 0, ulsch_DTX 0, BLER 0.00203 MCS (0) 0 (Qm 2 deltaMCS 0 dB) NPRB 5  SNR 50.5 dB CCE fail 0
UE 8e17: MAC:    TX            68 RX            787 bytes
UE 8e17: LCID 1: TX             3 RX             41 bytes
UE RNTI 9777 CU-UE-ID 3 in-sync PH 48 dB PCMAX 20 dBm, average RSRP -44 (16 meas)
UE 9777: dlsch_rounds 4/0/0/0, dlsch_errors 0, pucch0_DTX 0, BLER 0.08100 MCS (0) 0 CCE fail 2
UE 9777: ulsch_rounds 30/0/0/0, ulsch_errors 0, ulsch_DTX 0, BLER 0.00646 MCS (0) 0 (Qm 2 deltaMCS 0 dB) NPRB 5  SNR 50.5 dB CCE fail 0
UE 9777: MAC:    TX            51 RX            600 bytes
UE 9777: LCID 1: TX             3 RX             41 bytes
UE RNTI e013 CU-UE-ID 4 in-sync PH 48 dB PCMAX 20 dBm, average RSRP -44 (16 meas)
UE e013: dlsch_rounds 4/0/0/0, dlsch_errors 0, pucch0_DTX 0, BLER 0.08100 MCS (0) 0 CCE fail 8
UE e013: ulsch_rounds 31/0/0/0, ulsch_errors 0, ulsch_DTX 0, BLER 0.00646 MCS (0) 0 (Qm 2 deltaMCS 0 dB) NPRB 5  SNR 50.5 dB CCE fail 28
UE e013: MAC:    TX            51 RX            571 bytes
UE e013: LCID 1: TX             3 RX             49 bytes
```

(a) Before cell switching.

```
[0m[NR_MAC] Frame.Slot 256.0
UE RNTI a298 CU-UE-ID 1 in-sync PH 48 dB PCMAX 20 dBm, average RSRP -44 (16 meas)
UE a298: dlsch_rounds 8/0/0/0, dlsch_errors 0, pucch0_DTX 0, BLER 0.05314 MCS (0) 0 CCE fail 6
UE a298: ulsch_rounds 72/0/0/0, ulsch_errors 0, ulsch_DTX 0, BLER 0.00008 MCS (0) 0 (Qm 2 deltaMCS 0 dB) NPRB 5  SNR 50.5 dB CCE fail 0
UE a298: MAC:    TX           119 RX           1314 bytes
UE a298: LCID 1: TX             3 RX             41 bytes
UE RNTI 8e17 CU-UE-ID 2 in-sync PH 48 dB PCMAX 20 dBm, average RSRP -44 (16 meas)
UE 8e17: dlsch_rounds 8/0/0/0, dlsch_errors 0, pucch0_DTX 0, BLER 0.05314 MCS (0) 0 CCE fail 7
UE 8e17: ulsch_rounds 67/0/0/0, ulsch_errors 0, ulsch_DTX 0, BLER 0.00013 MCS (0) 0 (Qm 2 deltaMCS 0 dB) NPRB 5  SNR 50.5 dB CCE fail 0
UE 8e17: MAC:    TX           119 RX           1229 bytes
UE 8e17: LCID 1: TX             3 RX             41 bytes
UE RNTI 9777 CU-UE-ID 3 in-sync PH 48 dB PCMAX 20 dBm, average RSRP -44 (16 meas)
UE 9777: dlsch_rounds 7/0/0/0, dlsch_errors 0, pucch0_DTX 0, BLER 0.05905 MCS (0) 0 CCE fail 5
UE 9777: ulsch_rounds 56/0/0/0, ulsch_errors 0, ulsch_DTX 0, BLER 0.00042 MCS (0) 0 (Qm 2 deltaMCS 0 dB) NPRB 5  SNR 50.5 dB CCE fail 0
UE 9777: MAC:    TX           102 RX           1042 bytes
UE 9777: LCID 1: TX             3 RX             41 bytes
UE RNTI e013 CU-UE-ID 4 in-sync PH 48 dB PCMAX 20 dBm, average RSRP -44 (16 meas)
UE e013: dlsch_rounds 7/0/0/0, dlsch_errors 0, pucch0_DTX 0, BLER 0.05905 MCS (0) 0 CCE fail 17
UE e013: ulsch_rounds 57/0/0/0, ulsch_errors 0, ulsch_DTX 0, BLER 0.00042 MCS (0) 0 (Qm 2 deltaMCS 0 dB) NPRB 5  SNR 50.5 dB CCE fail 54
UE e013: MAC:    TX           102 RX           1013 bytes
UE e013: LCID 1: TX             3 RX             49 bytes
UE RNTI 2a67 CU-UE-ID 5 in-sync PH 48 dB PCMAX 20 dBm, average RSRP -44 (16 meas)
UE 2a67: dlsch_rounds 4/0/0/0, dlsch_errors 0, pucch0_DTX 0, BLER 0.08100 MCS (0) 0 CCE fail 3
UE 2a67: ulsch_rounds 27/0/0/0, ulsch_errors 0, ulsch_DTX 0, BLER 0.00886 MCS (0) 0 (Qm 2 deltaMCS 0 dB) NPRB 5  SNR 50.5 dB CCE fail 0
UE 2a67: MAC:    TX            51 RX            549 bytes
UE 2a67: LCID 1: TX             3 RX             41 bytes
UE RNTI 9511 CU-UE-ID 6 in-sync PH 48 dB PCMAX 20 dBm, average RSRP -44 (16 meas)
UE 9511: dlsch_rounds 4/0/0/0, dlsch_errors 0, pucch0_DTX 0, BLER 0.08100 MCS (0) 0 CCE fail 6
UE 9511: ulsch_rounds 27/0/0/0, ulsch_errors 0, ulsch_DTX 0, BLER 0.00886 MCS (0) 0 (Qm 2 deltaMCS 0 dB) NPRB 5  SNR 50.5 dB CCE fail 23
UE 9511: MAC:    TX            51 RX            549 bytes
UE 9511: LCID 1: TX             3 RX             41 bytes
```

(b) After cell switching.

Figure A.1 OAI gNB logs before and after cell switching, illustrating UE reassociation and connection preservation in the proposed framework.